

AD-A209 612

FILE COPY

2

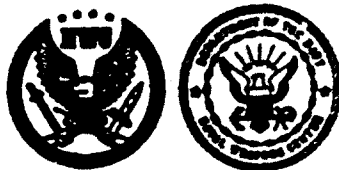
FWC TP 6945

Energetic Polyoxetane Thermoplastic Elastomers: Synthesis and Characterization

by
Geoffrey A. Lindsay, Mostafa A. H. Talukder, Robin A. Nissan,
Roxanne L. Quintana, Michael A. S. Hasting, Rena Y. Yee,
Melvin P. Nadler, Alice L. Arwood, and Russell Reed
Research Department
and
Gerald E. Manser
Aerojet Solid Propulsion Company
Sacramento, California

DECEMBER 1988

**NAVAL WEAPONS CENTER
CHINA LAKE, CA 93555-6001**



Approved for public release; distribution is unlimited.

SOT CD
ELEC E
JUL 01 89

HC H

89

1 0 0 0 2

Naval Weapons Center

FOREWORD

Polymeric binders are critically important ingredients in explosives and solid rocket propellants. Conventional binders are reactive liquid polymers which must be chemically crosslinked by special curing agents. These formulations are cured for many hours or days to develop the final properties. Many laboratories are evaluating thermoplastic elastomers (TPE) as low cost binders for formulations that can be extruder-mixed, continuously processed, and that require no cure. Thermoplastic elastomers may also improve ruggedness, stowage safety, and ease of demilitarization in future formulations. This report summarizes fiscal year 1987 work on developing new, energetic oxetane TPEs in collaboration with the Aerojet Solid Propulsion Co., Sacramento, Calif. New analytical techniques were developed for structure-property correlations. In fiscal year 1987, more than 30 different TPEs were prepared and characterized in detail.

This work was supported by Naval Weapons Center Independent Research funds, by the Office of Naval Research (R. S. Miller), and by the Strategic Defense Initiative Office/IST, Program Element number 63320C, Project Number 63320, Task RDDA, and Work Unit Number 138556.

This report has been reviewed for technical accuracy by Ronald L. Atkins and James M. Hoover.

Approved by
R. L. DERR, *Head*
Research Department
27 December 1988

Under authority of
J. A. BURT
Capt., USN
Commander

Released for publication by
G. R. SCHIEFER
Technical Director

NWC Technical Publication 6945

Published by.....Technical Information Department
Collation.....Cover, 39 Leaves
First printing.....165 Copies

UNCLASSIFIED

SECURITY CLASSIFICATION OF THIS PAGE

REPORT DOCUMENTATION PAGE

1a. REPORT SECURITY CLASSIFICATION UNCLASSIFIED		1b. RESTRICTIVE MARKINGS	
2a. SECURITY CLASSIFICATION AUTHORITY		3. DISTRIBUTION / AVAILABILITY OF REPORT Approved for public release; distribution is unlimited.	
2b. DECLASSIFICATION / DOWNGRADING SCHEDULE		4. PERFORMING ORGANIZATION REPORT NUMBER(S) NWC TP 6945	
5. MONITORING ORGANIZATION REPORT NUMBER(S)		6a. NAME OF PERFORMING ORGANIZATION Naval Weapons Center	
6b. OFFICE SYMBOL (if applicable)		7a. NAME OF MONITORING ORGANIZATION	
6c. ADDRESS (City, State, and ZIP Code) China Lake, CA 93555		7b. ADDRESS (City, State, and ZIP Code)	
8a. NAME OF FUNDING / SPONSORING ORGANIZATION Office of Naval Research		8b. OFFICE SYMBOL (if applicable) 1132P	
8c. ADDRESS (City, State, and ZIP Code) Arlington, VA 22217-5000		9. PROCUREMENT INSTRUMENT IDENTIFICATION NUMBER	
10. SOURCE OF FUNDING NUMBERS			
PROGRAM ELEMENT NO. 63220C	PROJECT NO. 63220	TASK NO. RDDA	WORK UNIT ACCESSION NO. 138556
11. TITLE (Include Security Classification) ENERGETIC POLYOXETANE THERMOPLASTIC ELASTOMERS: SYNTHESIS AND CHARACTERIZATION			
12. PERSONAL AUTHOR(S) Geoffrey A. Lindsay, et al.			
13a. TYPE OF REPORT Progress	13b. TIME COVERED FROM 86 Oct TO 87 Sep	14. DATE OF REPORT (Year, Month, Day) 1988, December	15. PAGE COUNT 76
16. SUPPLEMENTARY NOTATION			
17. COSATI CODES		18. SUBJECT TERMS (Continue on reverse if necessary and identify by block number)	
FIELD	GROUP	SUB-GROUP	Energetic Thermoplastic Elastomers, TPE, Polyoxetanes, GPC, NMR, Crystallization Rates
11	09		
20	08		
19. ABSTRACT (Continue on reverse if necessary and identify by block number) This report summarizes our work at the Naval Weapons Center developing improved polymeric binders for energetic materials during Fiscal Year 1987. Work focused on developing energetic oxetane thermoplastic elastomers (TPE) in collaboration with the Aerojet Solid Propulsion Co., Sacramento, Calif. Energetic TPEs were synthesized by sequential addition of monomers to a difunctional catalyst. Thermoplastic elastomer gumstocks were prepared with the following properties: melting temperatures high enough for useful mechanical properties and low enough for safe processing (70 to 85°C); crystallization rates of 5 to 10 minutes at room temperature; glass transition temperatures of -35 to -45°C; controllable molecular weights from 20 000 to 200 000 g/m; and, in many cases, molecular weight distributions of 1.3 to 1.5. Analytical techniques were developed and have provided partial understanding of the polymerization mechanism. Nuclear magnetic resonance measurements showed that certain reaction conditions result in the desirable block arrangement of monomer units. Crystallization rates of the hard segments and low temperature flexibility limits of the soft segments were measured by Fourier transform infrared and Differential Scanning Calorimetry. Since these measurements require very small samples (one gram), the cost of screening new polymer structures is lowered.			
20. DISTRIBUTION / AVAILABILITY OF ABSTRACT <input checked="" type="checkbox"/> UNCLASSIFIED/UNLIMITED <input type="checkbox"/> SAME AS RPT <input type="checkbox"/> DTIC USERS		21. ABSTRACT SECURITY CLASSIFICATION UNCLASSIFIED	
22a. NAME OF RESPONSIBLE INDIVIDUAL Geoffrey A. Lindsay		22b. TELEPHONE (Include Area Code) 619-939-1630	22c. OFFICE SYMBOL 3858

DD FORM 1473, 84 MAR

83 APR edition may be used until exhausted.

All other editions are obsolete

SECURITY CLASSIFICATION OF THIS PAGE

© U.S. Government Printing Office: 1986-607-044

UNCLASSIFIED



NWC TP 6945

CONTENTS

Accession For	
NTIS GRA&I	<input checked="" type="checkbox"/>
DTIC TAB	<input type="checkbox"/>
Unannounced	<input type="checkbox"/>
Justification	
By	
Distribution/	
Availability Codes	
Dist	Avail and/or Special
A-1	

Introduction..... 3

Synthesis and the Preliminary Analysis of 3,3'-Bis(azidomethyl)-oxetane, 3-Nitratomethyl-3'-methyloxetane, 3,3'-Bis(azidomethyl)-oxetane (BAMO-NMMO-BAMO) Triblock Copolymer..... 5

 Introduction..... 5

 Approach..... 5

 Structural Model..... 6

 Experimental Section..... 7

 Materials..... 7

 Procedure..... 7

 Results and Discussion..... 8

 Conclusion..... 15

Composition and Sequence Distribution by NMR..... 17

 Introduction..... 17

 Experimental Section..... 18

 Results and Discussion..... 19

¹H NMR..... 21

¹³C NMR..... 22

 Conclusions and Future Work..... 29

Molecular Weights, Molecular Weight Distributions, and Thermal Analysis by DSC..... 31

 Introduction..... 31

 Theoretical Background..... 31

 Results..... 35

 Experimental Section..... 37

 Materials..... 37

 Procedure..... 37

 GPC-LALLS..... 37

 Thermal Analysis..... 38

 Results and Discussion..... 38

 GPC-LALLS..... 38

 Thermal Analysis..... 40

 Conclusions..... 43

NWC TP 6945

Utility of Thermal and Structural Information.....45

- Introduction.....45
- Experimental Section.....45
- Discussion.....45
 - Glass Transition Temperature.....45
 - Melting Temperature.....47
 - Heat of Melting.....49
- Crystallization From the Melt.....50
- Results and Discussion.....50
 - Comparison of Different Types of Copolymers.....51
 - Comparison of B-A-B Polymers (Samples 727-4
Versus Sample 727-7).....52
 - Comparison of B-(B/A)-B (Sample 727-2
Versus Sample 727-3).....53
 - Comparison of Different Amounts of BAMO in Center
Block (Sample 646-79B Versus Sample 727-2).....53
 - Comparison of Different Center Blocks
(Sample 727-3 Versus Sample 727-9).....53
- Conclusions.....53

Composition and Crystallization by FT-IR.....55

- Introduction.....55
- Experimental Section.....55
- Results and Discussion.....56
 - Vibrational Assignments.....56
 - Crystallization Kinetics.....58
 - Block Identification.....64
- Conclusion.....65

Solid Rocket Propellant I_{sp} Calculations; Mechanical Properties.....67

- Introduction.....67
- Experimental Section.....67
- Results.....68
- Conclusions.....69

References.....71

INTRODUCTION

Novel energetic thermoplastic elastomer (TPE) binders are being explored and characterized in many government and industrial laboratories in an attempt to lower processing costs, improve ruggedness and stowage safety, and increase energetic content in future solid rocket propellants and explosive formulations.

Conventional binders, namely reactive liquid polymers, must be chemically crosslinked by special curing agents. These formulations are cured for many hours or days to develop the final properties. Thermoplastic elastomers contain "hard" segments that act as virtual crosslinking sites and "soft" segments that remain elastomeric and impart ruggedness and extensibility to the energetic material. We are focusing on hard segments (3,3'-bis(azidomethyl)-oxetane (BAMO)) and soft segments (3-azidomethyl-3'-methyloxetane (AMMO) and 3-nitratomethyl-3'-methyloxetane (NMMO)).

In order to mix the other ingredients into the final formulation, hard segments of the TPEs are softened by heating above their melting temperature. When the formulation is cooled to room temperature, the hard segments recrystallize to form virtual crosslinks, which impart the necessary physical strength to the propellant or explosive. Processing cycle times are greatly reduced, and problems of limited pot life are eliminated.

At the end of their unused life, propellants and explosives made from TPEs can be demilitarized by heating above the softening point of the TPE. In this molten state, the TPE can be removed more easily than conventional, chemically crosslinked formulations, and some of the ingredients may be recovered and recycled.

An energetic binder, which has nitrate or azido groups attached to the soft segment, can be used in larger amounts without penalizing the energy content of the formulation. Increasing the level of elastomer in energetic formulations will ruggedize the material. Since the hard segments of a TPE take up space that would ordinarily be occupied by highly energetic crystalline solids, the hard segments should be energetic themselves in order to maintain the energetic figures of merit of the formulations.

This report covers the first full year of work with Aerojet Solid Propulsion Co., Sacramento, Calif., to explore the feasibility of synthesizing polyoxetane block copolymers by means of the dicumyl chloride/silver hexafluoroantimonate (AgSbF₆) initiator system. The initial feasibility of polymerizing

NWC TP 6945

BAMO and NMMO was established in December 1986 at the Naval Weapons Center (NWC). Aerojet has been providing BAMO-b-AMMO-b-BAMO and BAMO-b-AMMO-co-BAMO-b-AMMO polymers made by this initiator system, and NWC has been characterizing these polymers.

In fiscal year 1987 more than 30 different TPEs were prepared and characterized in detail. We are investigating the microstructures and will be correlating these data with mechanical properties and processability.

This progress report is a compilation of reports that have been written by investigators working on the project.

SYNTHESIS AND THE PRELIMINARY ANALYSIS OF 3,3'-BIS(AZIDOMETHYL)-
OXETANE, 3-NITRATOMETHYL-3'-METHYLOXETANE, 3,3'-BIS(AZIDOMETHYL)-
OXETANE (BAMO-NMMO-BAMO) TRIBLOCK COPOLYMER

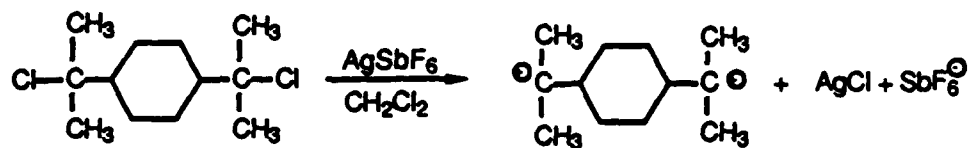
Mostafa A. H. Talukder, Investigator

INTRODUCTION

Attempts have been made to prepare energetic TPEs by cationic polymerization using cyclic ethers such as oxetanes (References 1). The conventional proton-oxonium ion mechanism has been tried without significant success. The stability of the propagating chains is one of the key points in the preparation of a block copolymer. If the propagating chain with cationic site is sufficiently stable (i.e., "living"), a homopolymer block of the first monomer is formed. As the propagating chain is still alive, a second monomer can be added to prepare another homopolymer block, and the process can be contained as long as monomer is fed to the system. Recently, carbocationic polymerization has been established as a living polymerization technique to prepare block copolymers (References 2 through 7). Although the present case is not a true carbocationic mechanism in that it involves polymerization of heterocyclic molecules such as oxetanes, we assume that a suitable carbonium ion initiator may generate a carbo-oxonium ion which might be more stable than a proton-oxonium ion. With this understanding in mind, the polymerization of cyclic ethers such as different oxetane derivatives has been undertaken with a special catalyst to prepare triblock copolymers. The overall purpose of this research program is to prepare a TPE with controlled molecular weight, functionality, block length, and block segments. As the polymerization system is conditioned to be living or quasi-living, the objectives should be achieved. Commercially available TPEs are not suitable for binding solid rocket propellants; they are not only nonenergetic but lack the proper fluid behavior at safe temperatures. When highly plasticized, commercially available TPEs also lack the necessary physical properties. The present polymerization process will help tailor the physicochemical and thermo-mechanical properties of the polymers to fit the desired application of the end product.

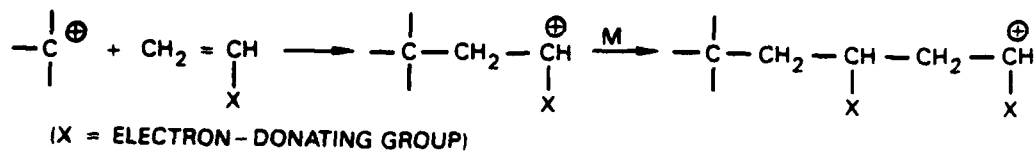
APPROACH

A difunctional initiator, *p*-bis(α,α -dimethylchloromethyl)benzene (*p*-DCC), is allowed to react with a cocatalyst, AgSbF_6 , to generate a carbonium ion (Reference 3), which subsequently starts polymerization of oxetane mono-mers through the formation of the carbo-oxonium ion.

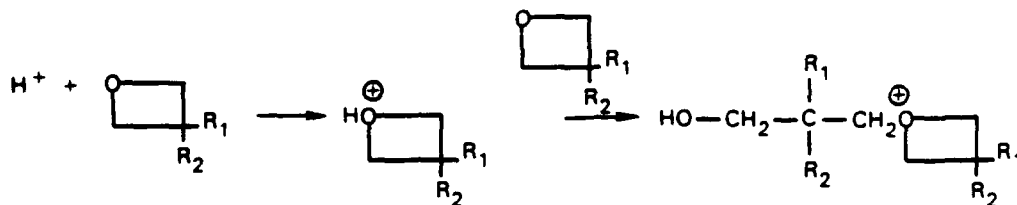


The mechanism of polymerization by the carbo-oxonium ion is shown in Figure 1 along with the carbo-cationic and proton-oxonium ionic mechanisms.

CARBOCATION



PROTON-OXONIUM



CARBO-OXONIUM

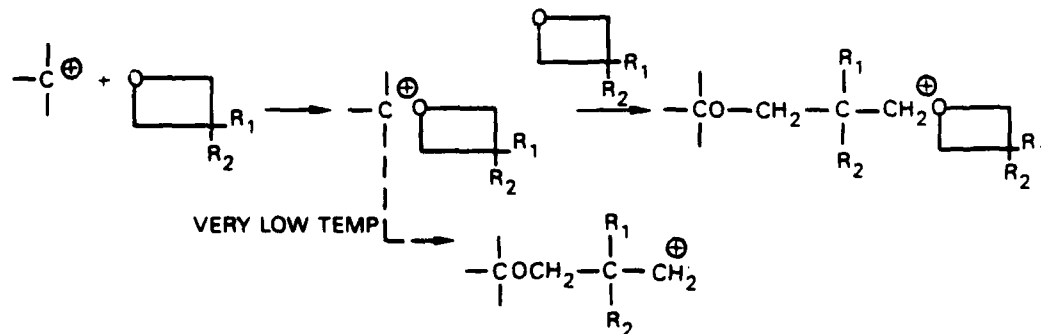


FIGURE 1. Mechanism of Polymerization.

STRUCTURAL MODEL

The structural model of triblock BAMO-NMMO-BAMO copolymer is shown in Figure 2. The difunctional initiator *p*-DCC was incorporated in the polymer. The use of a difunctional initiator offers the advantage of making a telechelic

polymer. Note that if the polymer is not intended to be used as a prepolymer, then a monofunctional initiator can be used in the same way to make a triblock copolymer. The only difference is that the initiator, instead of incorporating in the middle of the polymer, will be at the end of the polymer. The formation of a triblock copolymer should not be affected in any way assuming there is no chain transfer.

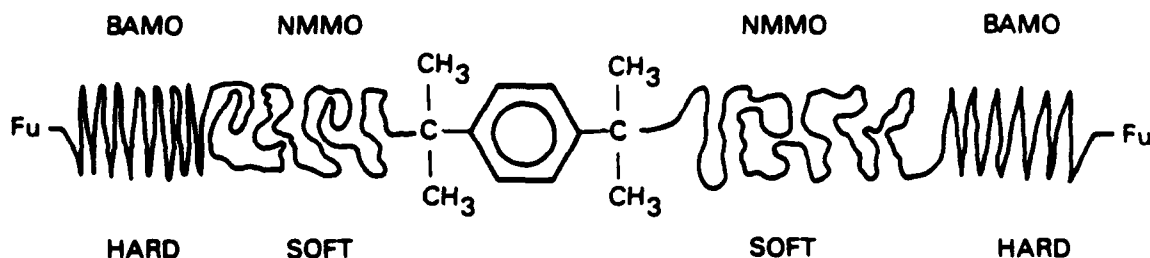


FIGURE 2. Structural Model of Triblock BAMO-NMMO-BAMO Copolymers.

EXPERIMENTAL SECTION

Materials

Bis(azidomethyl)oxetane was received from Aerojet, and the nitratomethyloxetane was prepared in our laboratory. Methylene chloride was distilled on calcium hydride and stored over molecular sieves. *p*-Bis(α,α -dimethylchloromethyl)benzene was prepared in the laboratory by passing hydrogen chloride gas through the methylene chloride solution of *p*-bis(isopropenyl)benzene at 0°C (Reference 4). The material was rotoevaporated, freeze-dried under vacuum, and stored under nitrogen. Silver hexafluoroantimonate was used as received from Aldrich Chemical Co., Milwaukee, Wis.

Procedure

A 300-mL three-necked Pyrex flask was flame-dried and charged with 20 mL of methylene chloride. The temperature of the solvent was maintained at -70°C under nitrogen. *p*-Bis(α,α -dimethylchloromethyl)benzene and AgSbF₆ were added to the reaction flask. The mixture was allowed to react for 1 to 5 minutes. Nitratomethyloxetane solution in methylene chloride was added slowly to the reaction flask, keeping the temperature of the reaction flask constant. To be sure that the NMMO was completely polymerized, the reaction mixture was allowed to react for 15 minutes. By taking samples periodically, the conversion was checked. Bis(azidomethyl)oxetane solution in methylene chloride was then added to the reaction flask in the same way as NMMO. After the complete addition of BAMO, the reaction mixture was allowed to stir for an additional period of time. The reaction was terminated with ammonium hydroxide. The organic layer was separated, concentrated, and mixed with

methanol. The white precipitate was dried under vacuum to give a rubbery polymer. The polymer was analyzed by nuclear magnetic resonance (NMR), infrared (IR), gel permeation chromatography-low angle laser light scattering (GPC-LALLS), and differential scanning calorimetry (DSC).

RESULTS AND DISCUSSION

The ^1H NMR spectra of *p*-diisopropenylbenzene and *p*-dicumyl chloride are shown in Figures 3 and 4, respectively. The doublet of *p*-diisopropenylbenzene (Figure 3) may be referred to as an indicator or monitor for the hydrochlorination of *p*-diisopropenylbenzene. The doublet peaks disappeared completely in Figure 4, indicating the completion of the reaction. The phenylene group of *p*-diisopropenylbenzene and *p*-dicumyl chloride appeared at 7.6 ppm. The methyl groups of *p*-dicumyl chloride showed a singlet peak at about 2.0 ppm. The integration ratio of the peak at 2.0 ppm and 7.6 ppm is about 3 within experimental error.

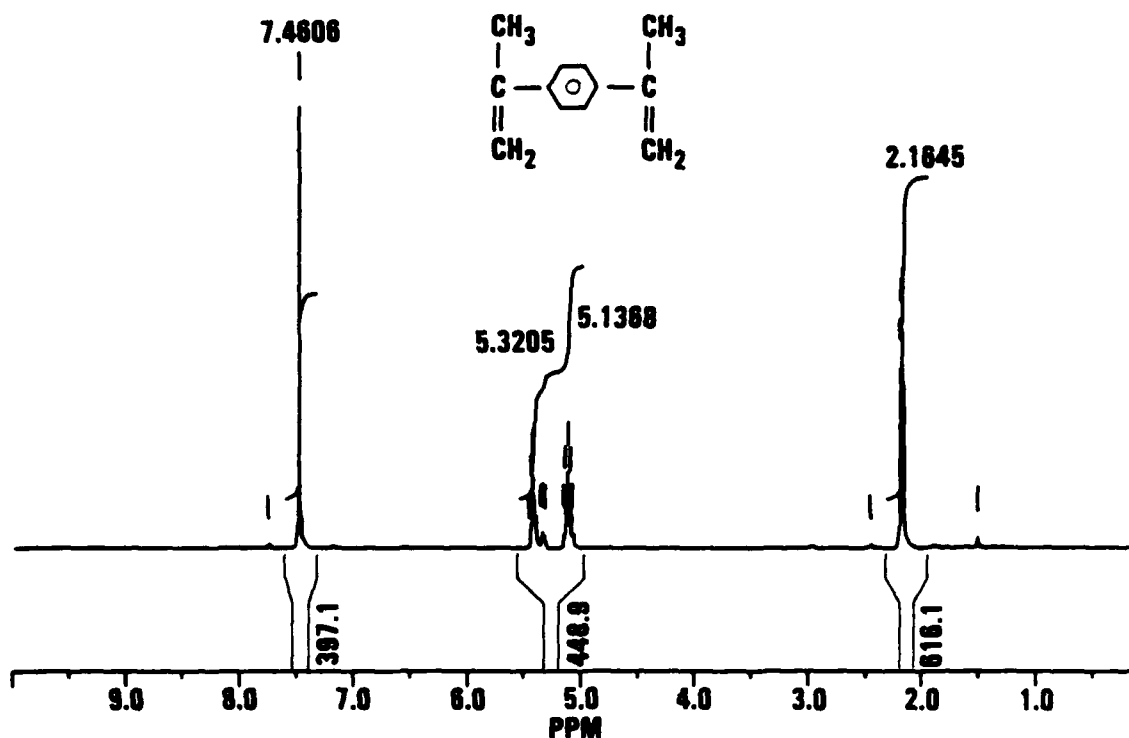


FIGURE 3. ^1H NMR Spectrum of *p*-Diisopropenylbenzene.

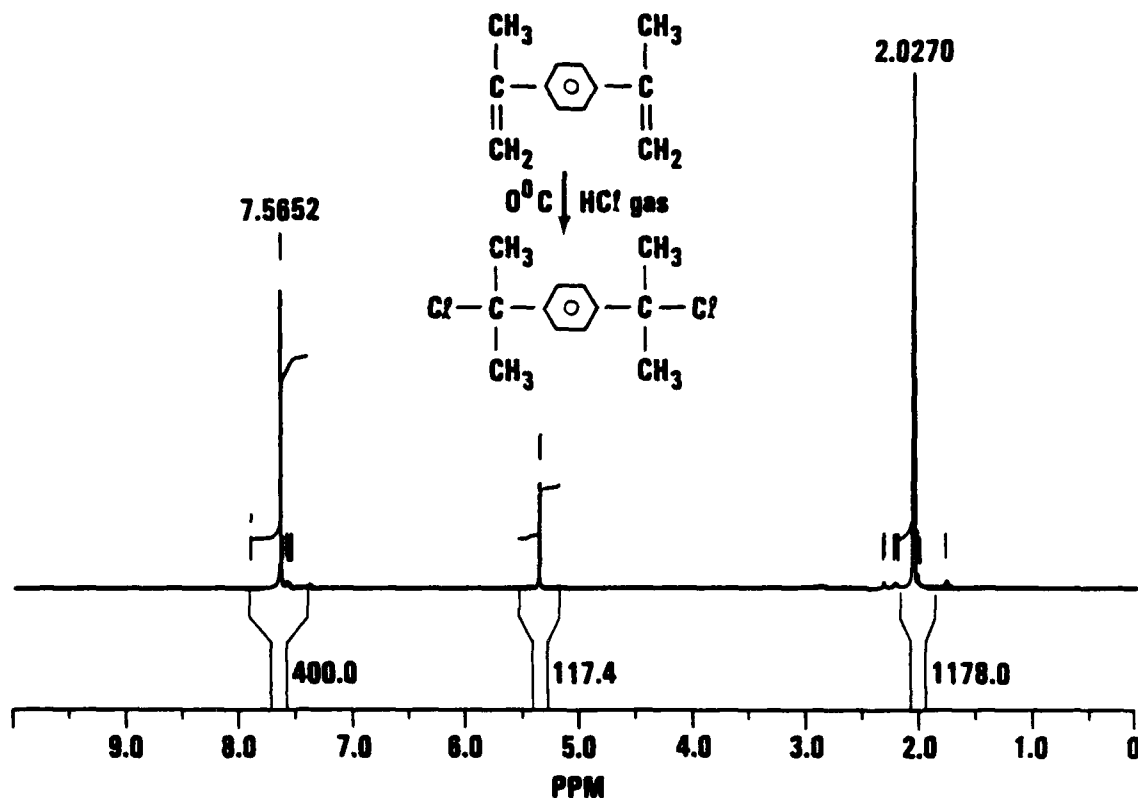


FIGURE 4. ^1H NMR Spectrum of *p*-Dicumyl Chloride.

The ^1H NMR spectrum of the copolymer (Figure 5) has been assigned by referring to spectra of the homopolymers of BAMO and NMMO (Figures 6 and 7). The side methylene groups ($-\text{CH}_2\text{ONO}_2$) of NMMO were shown at 4.3 to 4.4 ppm. The peaks at 3.1 to 3.3 ppm were assigned to main chain methylene groups of NMMO and BAMO including side chain methylene groups ($-\text{CH}_2\text{N}_3$) of BAMO. The peak at 0.9 ppm was assigned to a CH_3 group of NMMO. The phenylene fragment of *p*-DCC was shown at about 7.1 ppm. In the original spectrum, the peak is very weak due to the high molecular weight of the polymer. However, if the spectrum is magnified, then the peak is very clear as shown in Figure 3. The appearance of a phenylene fragment peak at 7.1 to 7.2 ppm is very significant indicating that both of the tertiary chlorine atoms have been cleared to give dicarbocations for initiation of polymerization from both ends of the catalyst (Reference 4).

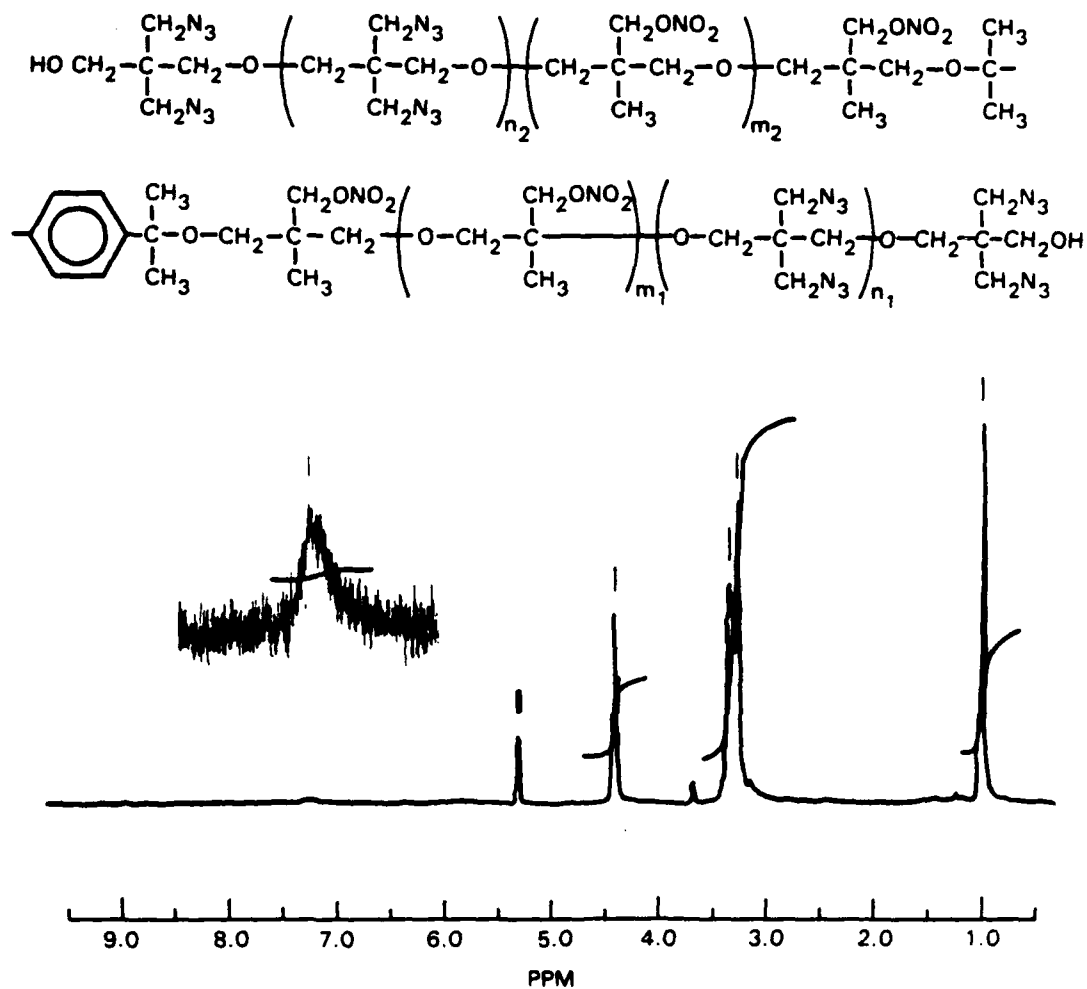


FIGURE 5. ^1H NMR Spectrum of BAMO-NMMO-BAMO Triblock Copolymer.

NWC TP 6945

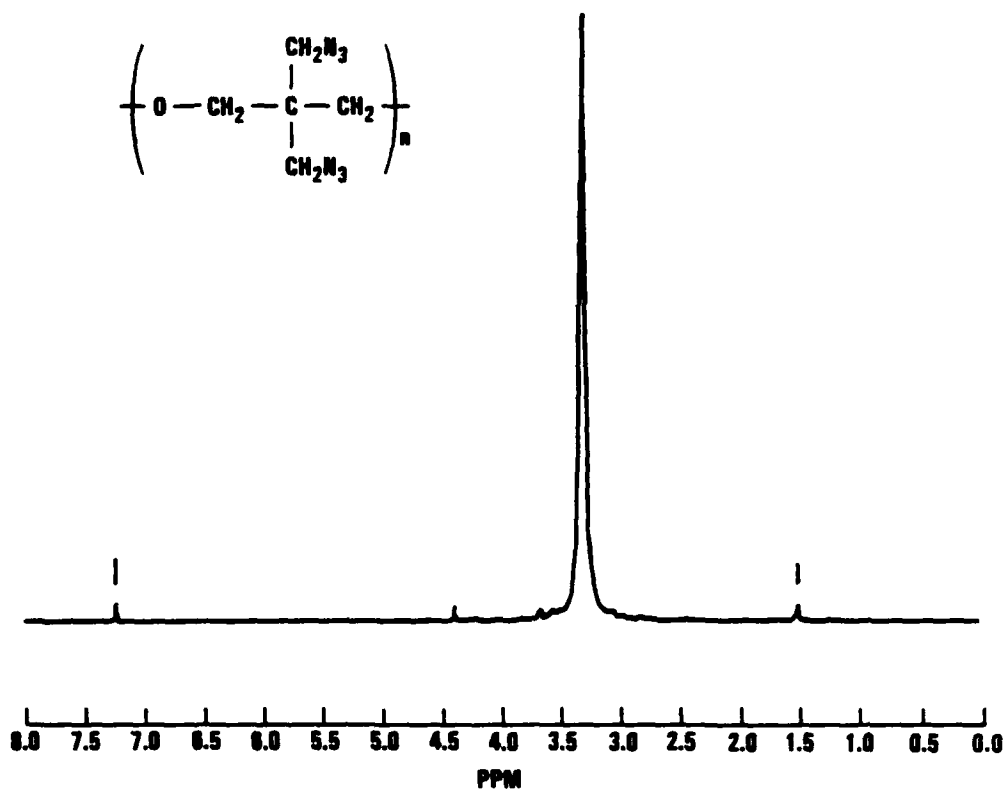


FIGURE 6. ¹H NMR Spectrum of PolyBAMO (CDCl₃).

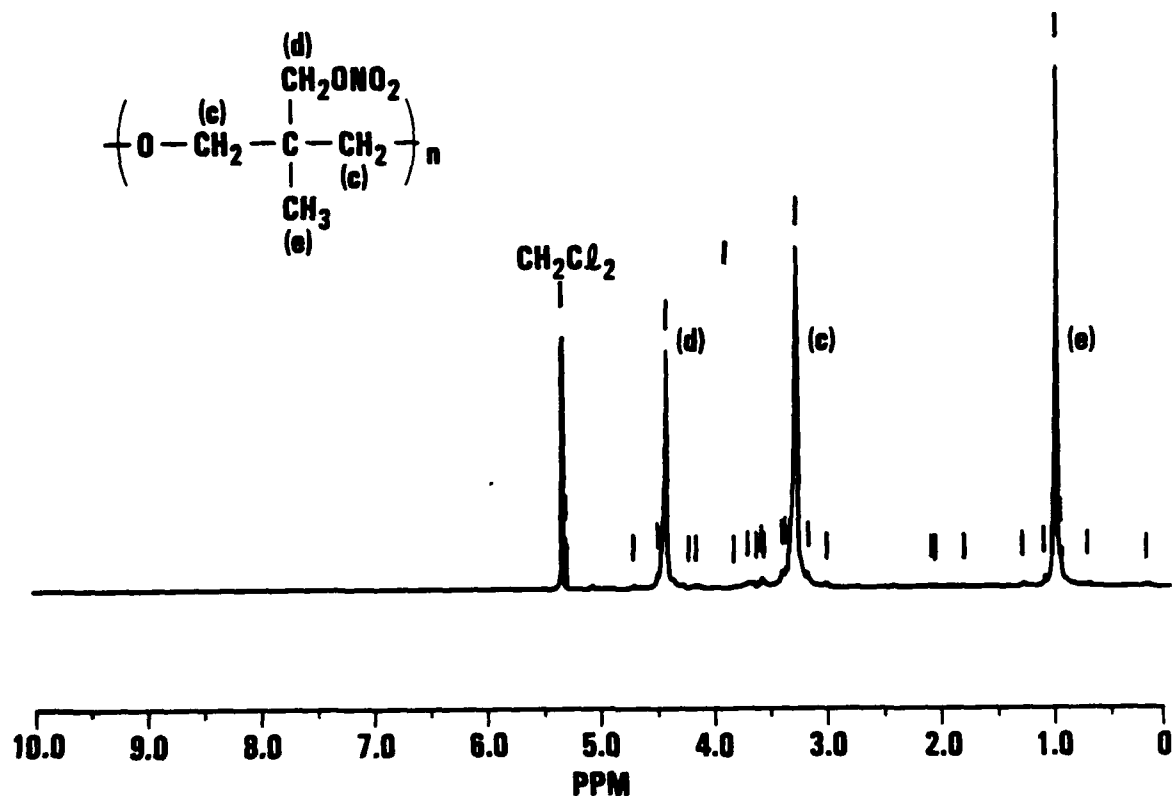


FIGURE 7. ^1H NMR Spectrum of PolyNMMO.

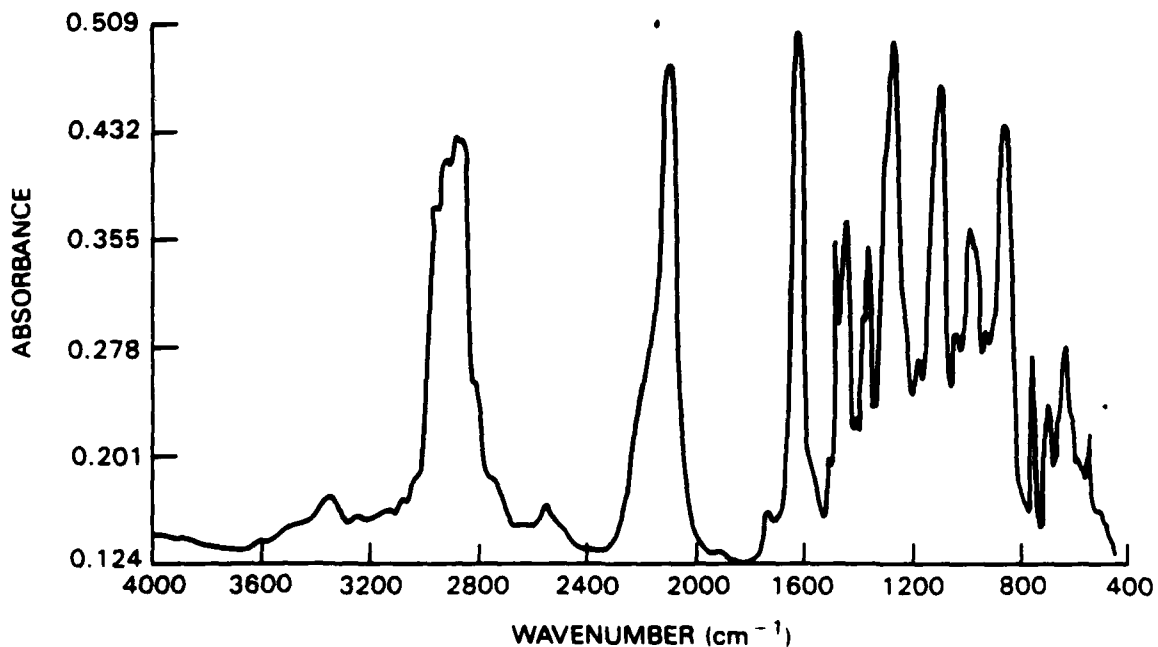


FIGURE 8. IR Spectrum of BAMO-NMMO-BAMO Triblock Copolymer.

The Fourier transform-infrared (FT-IR) spectrum of the polymer (Figure 8) shows a peak at 3610 cm^{-1} , which indicates the presence of free hydroxyl groups in the polymer. The peak at 572 cm^{-1} is the azide bend of crystalline BAMO. The GPC-LALLS chromatograms of the polymer are shown in Figure 9. The molecular weight distribution is narrow ($\bar{M}_w/\bar{M}_n = 1.3$) indicating that the polymerization is governed by a living or quasi-living ionic mechanism. The glass transition temperature (T_g) of the polymer as shown in Figure 10 is about -27°C ; the melting point is about 56°C . Note that, as expected, the T_g of the copolymer is close to that of polyNMMO. The decomposition point of the polymer, as measured by thermogravimetric analysis (TGA) (Figure 11), is 204°C , which indicates good thermal stability of the polymer.

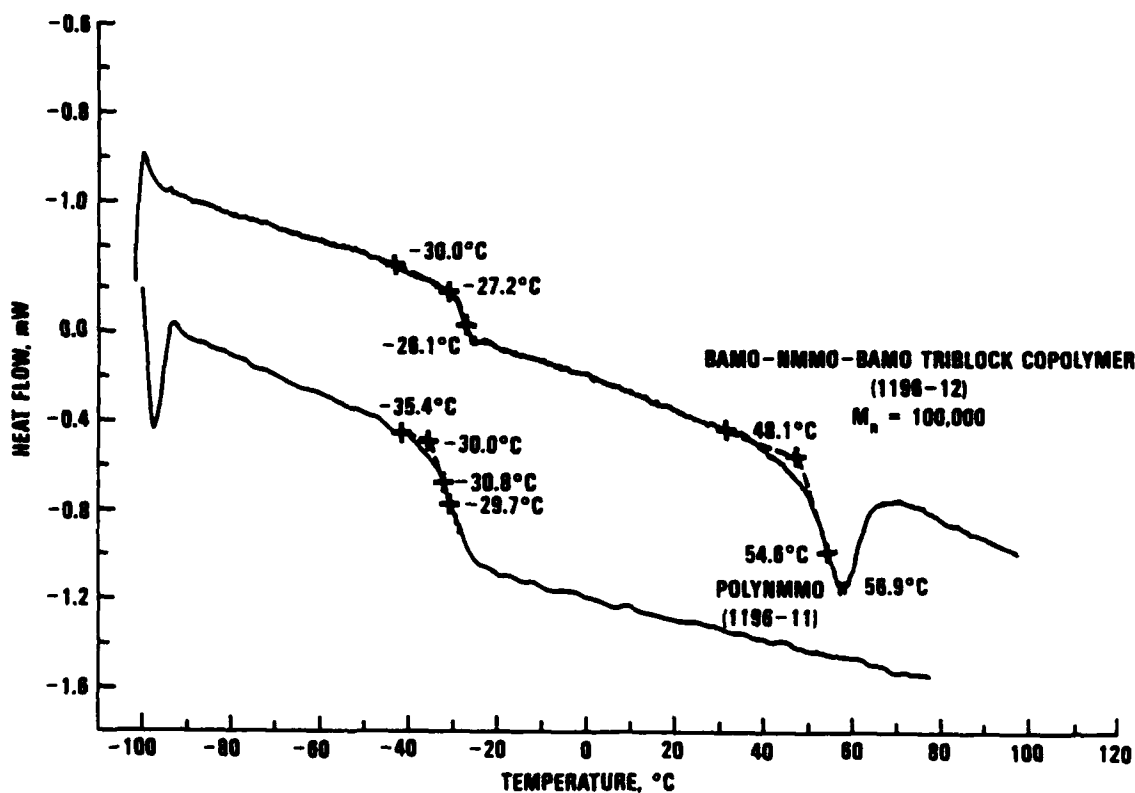


FIGURE 9. DSC Thermogram of Oxetane Polymers.

NWC TP 6945

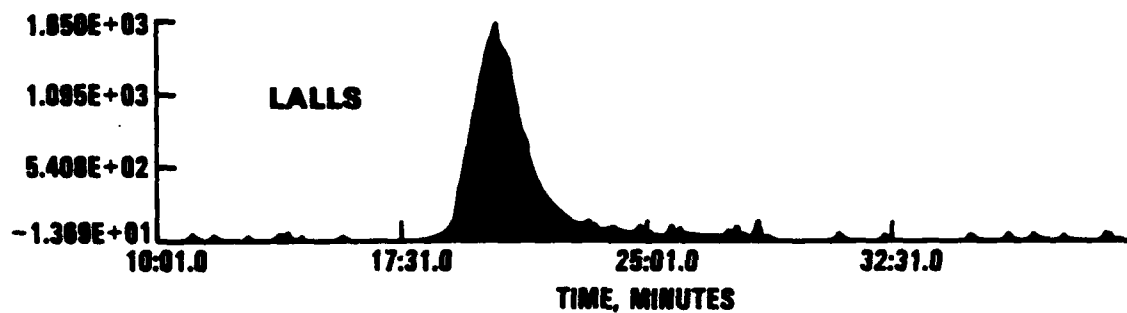
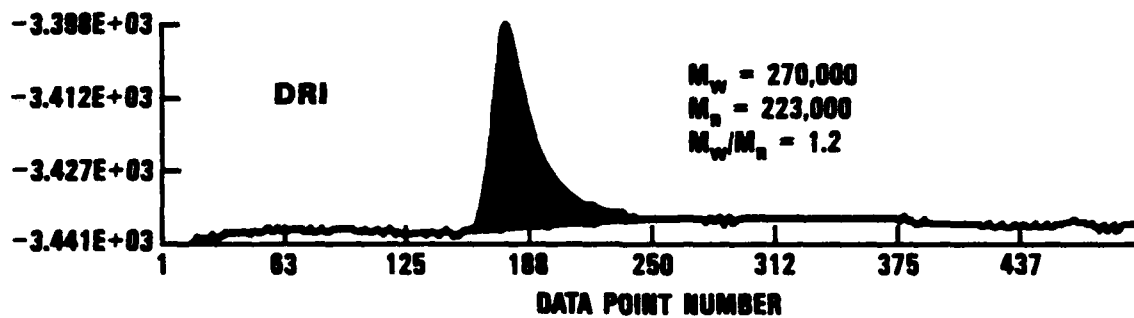


FIGURE 10. GPC-LALLS Chromatograms of BAMO-NMMO-BAMO Triblock Copolymer.

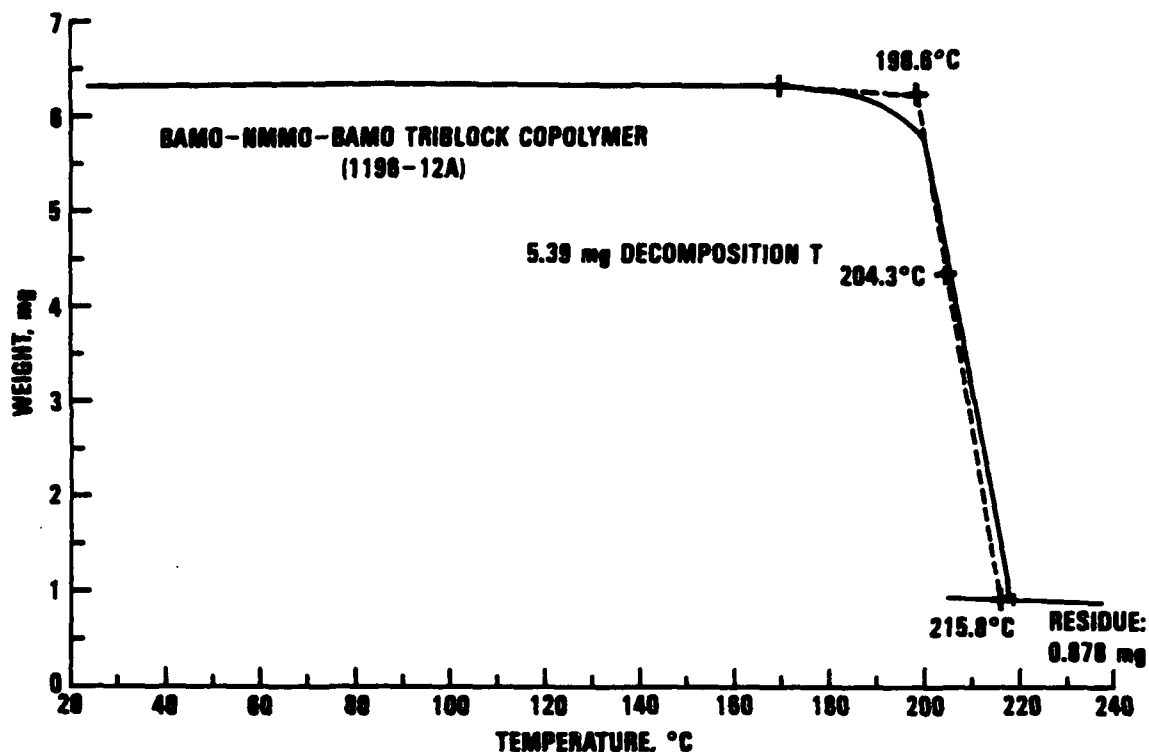


FIGURE 11. TGA Analysis of BAMO-NMMO-BAMO Triblock Copolymer.

CONCLUSION

The BAMO-NMMO-BAMO triblock copolymer has been prepared by cationic polymerization using a carbo-oxonium ion mechanism. The polymer is telechelic, i.e., contains hydroxyl terminal groups. The analyses of the polymer by different techniques such as NMR, FT-IR, GPC, and DSC show that the structure of the polymer agrees with the theoretical model. The concept of the preparation of triblock copolymers of cyclic ether monomers, especially oxetanes, using the *p*-DCC/AbSbF₆ initiator system has been proven. Further work is warranted to explore the system.

COMPOSITION AND SEQUENCE DISTRIBUTION BY NMR

Robin A. Nissan and Roxanne L. Quintana, Investigators

INTRODUCTION

Depending on the monomer feed strategy, sequential addition of AMMO and BAMO monomers allows for the formation of triblock polymers of the form BAMO-AMMO-BAMO (B-A-B) or BAMO-(BAMO/AMMO)-BAMO (B-(B/A)-B) (References 1). Structural analysis of these materials is essential in understanding the mechanism of polymerization. Furthermore, the information gained from an in-depth structural study can be used to improve the synthesis of materials that are tailored for specific formulations. Nuclear magnetic resonance techniques offer several unique advantages for the study of copolymers (Reference 8). In particular, a combination of ^1H and ^{13}C NMR spectroscopy can yield information on monomer incorporation, sequence distribution, reactivity ratios, and perhaps polymer morphology if detailed relaxation or variable temperature measurements are made. One major drawback in the quantitative study of macromolecules by NMR methods is that of dynamic range (Reference 9). It is often difficult to quantify end groups or initiators of very long chains using ^1H NMR methods; ^{13}C NMR methods suffer further in terms of dynamic range.

Analysis of bulk polymer microstructure by NMR methods is unsurpassed in its information content. Sequence distribution information is accessible in several of the polyoxetane systems we have studied, including random polyBAMO/NMMO, bisazidomethyloxetane/tetrahydrofuran (BAMO/THF) copolymers, and the BAMO-AMMO systems. In each case, triad distribution information is available in the ^{13}C NMR spectra (Figure 12). The quaternary ^{13}C resonances (45.4 and 41.3 ppm for BAMO/AMMO polymers) are most sensitive to nearest neighbor effects and are simple to analyze in terms of sequence distributions. The methylene ether main chain carbons also show splitting due to sequence distribution; however, the peak separations are small and only diad resonances are discernible. This section will deal with ^1H and ^{13}C NMR studies on the B-A-B and B-(B/A)-B systems. Experimental triad distributions are compared to those calculated for perfectly random or perfectly blocky polymers.

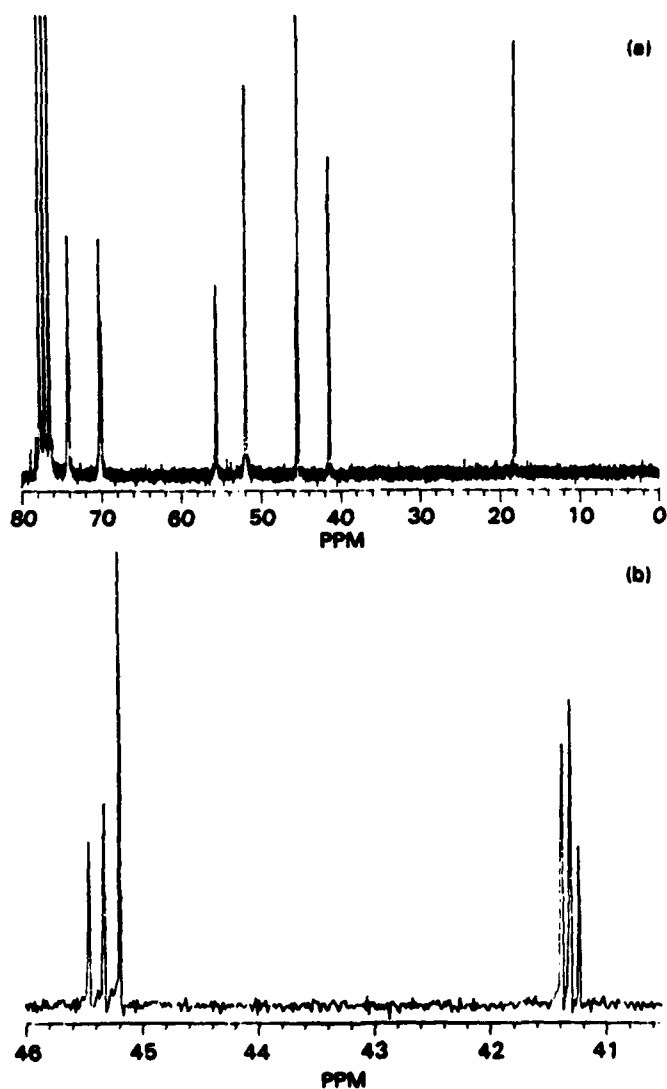


FIGURE 12. ^{13}C NMR Spectra of a BAMO/AMMO Copolymer for (a) Complete Spectrum, and (b) Quaternary Carbon Region.

EXPERIMENTAL SECTION

All oxetane polymers studied in this project, with the exception of one sample of random BAMO/AMMO (Rocketdyne, Azusa, Calif.), was prepared previously, with butanediol borontrifluoride etherate initiator) were prepared by Aerojet. ^1H and ^{13}C NMR spectra of polymer solutions in deuteriochloroform (CDCl_3), MSD Isotopes, Montreal, Quebec, Canada, were recorded on an IBM

AF/NR-80 spectrometer operating at 80 megahertz for ^1H NMR and 20 megahertz for ^{13}C NMR acquisition or on an NT-200 WB spectrometer operating at 200 megahertz for ^1H NMR and 50 megahertz for ^{13}C NMR acquisition. Quantitative ^{13}C NMR spectra were recorded under gated decoupling conditions (decoupler off prior to acquisition) with an 11.4 second recycle time and a pulse width of 45 degrees. Under these conditions all main chain, side chain, methyl, methylene, and quaternary carbon resonances were consistently quantifiable. Longer relaxation delays had no effect on integrations. Spectra were recorded for the individual homopolymers and for several random copolymers with differing co-monomer ratios. In order to assign all resonances, distortionless enhancement by polarization transfer (DEPT) (Reference 10) spectra were recorded. ^1H NMR spectra were acquired with 10-second recycle times and pulse widths of 30 degrees and were used to confirm monomer compositions; however, since all resonances were of similar widths and resonances of individual carbon types did not overlap, ^{13}C NMR data were considered more reliable.

RESULTS AND DISCUSSION

In the course of this work, we have analyzed more than 20 polymers of the form B-A-B or B-(B/A)-B. In addition, we have also studied several "random" B/A polymers. The samples were synthesized using varied experimental techniques designed to eventually optimize triblock formation. Initiator concentrations and mode of formation were varied. Rates of addition of monomer and ratios of co-monomers in random centerblocks were also varied so that the effect of these parameters on the isolated oxetane polymers could be judged. Our investigations on polymer microstructure, detailed in this report, are intended to supply useful information to the continuing synthetic program.

Table 1 is a list of the polymers we have studied and includes some information on molecular weights and polydispersities which we have measured by GPC-LALLS. In addition, \bar{M}_n s calculated from the ^1H NMR spectra are listed in Table 1. (Integrations of aromatic initiator resonances are compared to the main chain and side chain ^1H resonances for the polymer to yield an experimental \bar{M}_n .) These ^1H NMR values for \bar{M}_n are always lower than the GPC-LALLS values indicating higher than expected incorporation of initiator. Where available, information on mole ratios of monomers charged to the polymerization vessel in terms of hard and soft blocks is included. Note that percent conversion to polymer was reported to be $> 97\%$ for all polymerizations, and AMMO was always completely consumed while BAMO monomer was sometimes found in aliquots withdrawn from the polymerization vessel.

TABLE 1. Polymers Studied to Date Including Some Experimental Results

Sample designation	Compounds, ^a H-S-H	H-S-H molar composition	B/A composition, %	\bar{M}_n , K	\bar{M}_w/\bar{M}_n	Block factor ⁱ	Block Index ^c	¹ H NMR \bar{M}_n , K
646-79B	B-(B/A)-B	-	69/31	81	2.8	35	55	58
646-91A	B-(B/A)-B	0.08-0.22-0.08	69/31	181	3.4	47	66	73
646-94	B-(B/A)-B	0.03-0.112-0.03	69/31	72	1.3	29	48	133
646-95	B-(B/A)-B	0.025-0.112-0.025	76/24	59	1.2	20	45	107
646-98	B-(B/A)-B	0.07-0.34-0.07	68/32	-	-	29	50	98
646-99	B-(B/A)-B	0.06-0.28-0.06	66/34	56	1.2	39	61	50
727-2 ^d	B-(B/A)-B	-	53/47	84	1.5	28	67	28
727-3 ^d	B-(B/A)-B	0.06-0.10-0.06	51/49	61	1.2	34	68	59
727-10	B-(B/A)-B	0.048-0.22-0.048	66/34	34	1.7	25	47	33
727-11 ^e	B-(B/A)-B	0.055-0.26-0.055	65/35	33	1.5	28	49	-
727-12	B-(B/A)-B	0.024-0.114-0.024	73/27	-	-	15	41	29
727-13 ^d	B-(B/A)-B	0.025-0.114-0.025	57/43	-	-	30	47	35
727-14	B-(B/A)-B	0.048-0.22-0.048	66/34	-	-	28	48	-
727-16	B-(B/A)-B	0.048-0.22-0.048	65/35	-	-	30	50	30
727-17 ^d	B-(B/A)-B	0.06-0.23-0.06	50/50	-	-	21	62	39
Rocketdyne ^o	B/A	-	55/45	-	-	1	20	-
646-89	B/A	-	45/55	10	2.3	5	39	-
727-5	B/A	0.10/0.14	38/62	38	1.2	1	44	20
727-5B	B/A	0.14/0.14	52/48	53	1.2	17	45	33
727-4	B-A-B	0.048-0.24-0.048	23/77	60	1.2	13	86	31
727-7	B-A-B	0.031-0.16-0.031	26/74	23	1.6	12	77	24
727-9	B-A-B	0.048-0.12-0.048	45/55	38	1.2	26	77	26
727-18	B-A-B	0.055-0.25-0.055	29/71	42	2.3	20	89	29

^a (B/A) Centerblocks are 50% BAMO/50% AMMO unless otherwise noted.

^b BBB-(ABB)/2.

^c (BBB + AAA)/Total.

^d (B/A) Centerblock is 30% BAMO/70% AMMO.

^e Sample of BAMO/AMMO random polymer prepared by butanediol/BF etherate initiation.

Also included in Table 1 are a block factor and a block index. These numbers are derived from the integrated ¹³C NMR spectra. The block factor takes the integrated area of the BBB triad, and in an attempt to correct for BBB triads that are present in random segments of the polymer, one half of the integrated ABB triad is subtracted. This block factor is expected to reflect the percentage of BAMO that is present in hard block segments of the polymer. This block factor will be dependent upon the expected mole ratio of hard segment, that is, if the polymer was prepared such that 80% of the monomer was in the soft center block and 10% in each of the hard block end segments, then a block factor of 20 would be ideal. For higher concentrations of hard block, the ideal block factor increases proportionally. The block index is derived by adding together the BBB and AAA triads and dividing by the total area of all triads. This number is expected to reflect the overall polymer blockiness. For B-A-B polymers, the ideal triblock polymer will have a block index that approaches unity since there will only be two A-B diads per chain. For B-(B/A)-B polymers, the block index will be affected by center block composition and, therefore will not be a reliable indicator of triblock

formation. As the mole ratio of center block increases, the ideal block index will decrease. Additionally, changes in the BAMO to AMMO ratio in the center block or differences in the reactivity ratios of the two monomers may have a marked effect on the calculated block index since blockiness in the center block is included in this index.

¹H NMR

The ¹H NMR spectra of BAMO-AMMO polymers are not very informative (Figure 13). The AMMO methyl protons resonate at 0.95 ppm and all of the methylene protons (nitrate methylene, azidomethylene, and main chain ether methylenes) resonate near 3.25 ppm. In addition, we occasionally observe an exchangeable proton resonance near 1.5 ppm (addition of deuterium oxide to the samples leads to the broadening of the peak at 1.5 ppm). We believe that this resonance is related to the polymer end groups and to the hexafluoroantimonate (SbF₆⁻) which may hydrolyze upon workup. There is evidence of small concentrations of BAMO monomer (< 0.1%, proton resonances at 4.40 and 3.68 ppm) in just a few of the samples studied. Note also, that end group analysis by trifluoroacetylation indicates only BAMO-hydroxyl (OH) end groups for the most recent B-A-B polymers studied.

Resonances associated with the DCC initiator are observed near 7.33 and 1.50 ppm (assigned to the aromatic and methyl protons, respectively). The aromatic peaks near 7.33 ppm are integrated and compared to the monomer resonances to yield a value for \bar{M}_n . This number when compared to the GPC-LALLS \bar{M}_n is lower in most cases, indicating that the initiator is present in higher than expected concentrations. There are two examples (samples 646-94 and 646-95) where the ¹H NMR calculated molecular weight is much larger than the GPC-LALLS molecular weight. It should be noted that for these two spectra, the peaks associated with DCC initiator were just barely above noise level. In nearly all samples studied, there are several broad resonances in the region of 7.33 ppm indicating that the initiator is not a simple dicumyl species. Based on studies of polymer molecular weight versus initiator charge (measured molecular weights are generally three times the molecular weight expected), we conclude that the initiator may be self-polymerizing. Hydrogen chloride elimination would lead to reactive methyl styrene units. Presently, we find that ¹H NMR calculations of molecular weight are unreliable for this system.

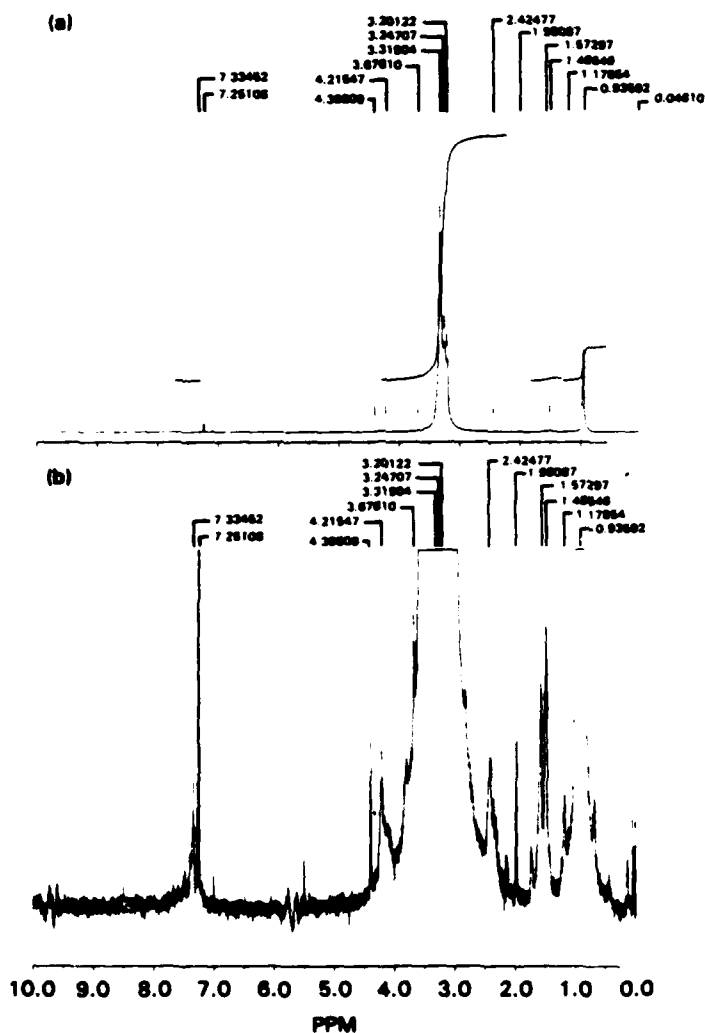


FIGURE 13. ^1H NMR Spectrum of a BAMO/AMMO Copolymer For (a) 0 to 10 ppm Region and (b) Expanded y Scale.

^{13}C NMR

Typical ^{13}C NMR spectra of a random B/A and of a B-(B/A)-B block polymer, where the center block is a 30/70 BAMO/AMMO random polymer, are displayed in Figure 14. These and a series of homopolymer spectra were used to make the assignments shown. Under the gated decoupling conditions employed, the integrated resonances are quantifiable and monomer distributions may be calculated.

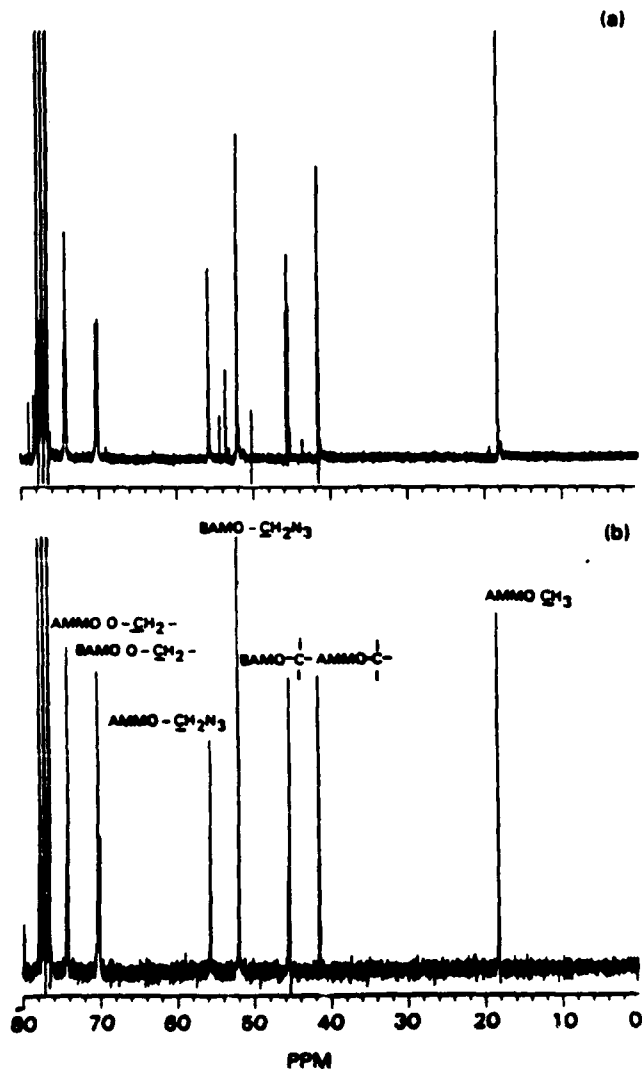


FIGURE 14. ^{13}C Spectra and Assignments For Random (a) B/A and Triblock and (b) B-(B/A)-B Polymers.

Of greater interest are the splittings observed in the quaternary carbon region displayed in Figure 15. The splitting of each peak into three separate resonances indicates that triad sequences are observed. The triad resonances have been assigned based on comparisons with homopolymers and based on studies of random polymers with differing ratios of comonomers. Integration of these separate resonances leads to a measurement of triad sequence distributions. These measurements are an accurate description of the polymer microstructure. Table 2 is a compilation of the integrated triad sequences normalized to 100 for several examples of the B/A, B-A-B, and B-(B/A)-B polymers prepared for this project. Also included in Table 2, where applicable, are calculations of triad distributions based either on a random polymerization mechanism with equal monomer reactivity ratios, or on an ideal triblock

polymerization mechanism. For the ideal triblock calculations, triad sequence distributions are obtained by adding the expected hard block BAMO charge to the calculated random center block derived based on equal reactivity ratios of the two monomers. Calculations for the B-A-B polymers are much more straightforward since they only involve BAMO and AMMO blocks and two B-A diads per chain.

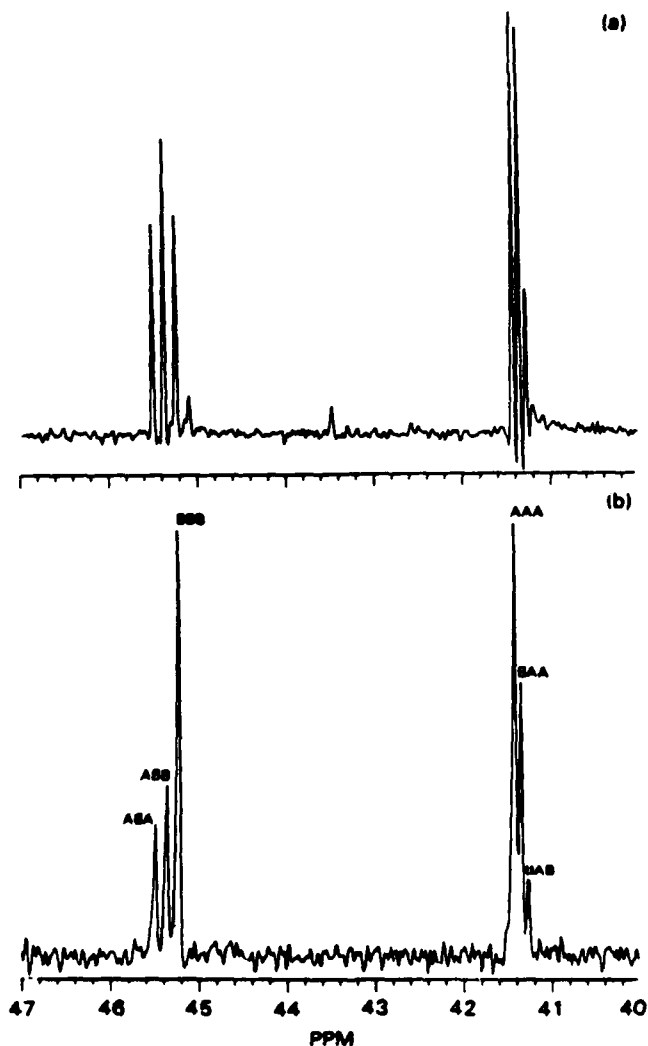


FIGURE 15. ^{13}C Spectra Expanded Quaternary Region For Random (a) B/A and Triblock (with resolution enhancement) and (b) B-(B/A)-B Polymers (without resolution enhancement).

Inspection of Table 2 leads to the conclusion that the B-A-B polymers are for the most part blocky polymers (generally better than 90% of the monomers are in blocky segments, although, more recently B-A-B polymers with greater than 97% blockiness have been studied). This same general con-

clusion can be made for the B-(B/A)-B polymers, though in some cases the evidence for blockiness is less compelling. The assumption of equal reactivity ratios for BAMO and AMMO monomers is based on work previously reported (Reference 1), however, this present work would tend to indicate that the two reactivity ratios differ significantly. Inspection of the experimental triad distributions found for sample 727-5B confirms this. Although the sample is nearly 50/50 BAMO/AMMO, there are disproportionate percentages of BBB and AAA triads.

Narrow polydispersities observed in the GPC-LALLS experiments serve to indicate that most of the polymers are indeed block polymers rather than mixtures of homopolyBAMO and random BAMO/AMMO or homopolyAMMO.

TABLE 2. Experimental and Calculated Triad Distributions.

Polymer	Experimental ^c	Calculated, ^{a,b} random	Calculated, ^{a,b} triblock
Sample 646-79B (B-B/A-B)			
ABA	7	7	8
ABB	18	29	15
BBB	44	33	46
AAA	11	3	8
BAA	13	13	15
BAB	7	15	8
Sample 646-91A (B-B/A-B)			
ABA	4	7	8
BBB	13	29	15
BBB	53	33	46
AAA	13	3	8
BAA	10	13	15
BAB	7	15	8
Sample 646-94 (B-B/A-B)			
ABA	8	6	8
ABB	21	29	15
BBB	40	33	46
AAA	8	3	8
BAA	12	13	15
BAB	11	15	8
Sample 646-95 (B-B/A-B)			
ABA	9	7	8
ABB	26	30	17
BBB	32	30	42
AAA	9	4	8
BAA	13	15	17
BAB	11	15	8

See footnotes at end of table.

NWC TP 6945

TABLE 2. (Contd.)

Polymer	Experimental ^c	Calculated, a,b random	Calculated, a,b triblock
Sample 646-98 (B-B/A-B)			
ABA	10	7	8
ABB	20	30	16
BBB	39	31	44
AAA	11	3	8
BAA	13	14	16
BAB	7	15	8
Sample 646-99 (B-B/A-B)			
ABA	7	8	9
ABB	13	29	17
BBB	46	29	40
AAA	15	4	9
BAA	14	15	17
BAB	5	15	9
Sample 727-2 ^d (B-B/A-B)			
ABA	8	12	10
ABB	11	26	8
BBB	34	15	35
AAA	33	10	23
BAA	11	24	20
BAB	3	13	3
Sample 727-3 ^d (B-B/A-B)			
ABA	5	12	10
ABB	8	26	9
BBB	38	13	32
AAA	30	12	24
BAA	13	24	21
BAB	6	13	4
Sample 727-10 (B-B/A-B)			
ABA	9	8	9
ABB	21	29	17
BBB	36	29	40
AAA	11	4	9
BAA	15	15	17
BAB	8	15	9
Sample 727-11 (B-B/A-B)			
ABA	7	8	9
ABB	20	30	17
BBB	38	27	39
AAA	11	4	9
BAA	15	16	17
BAB	9	15	9

See footnotes at end of table.

TABLE 2. (Contd.)

Polymer	Experimental ^c	Calculated, ^{a,b} random	Calculated, ^{a,b} triblock
Sample 727-12 (B-B/A-B)			
ABA	7	5	7
ABB	24	29	14
BBB	42	39	53
AAA	5	2	7
BAA	11	11	14
BAB	11	14	7
Sample 727-13 (B-B/A-B) (50/50%)			
ABA	10	11	11
ABB	21	28	22
BBB	26	19	25
AAA	15	8	11
BAA	20	21	22
BAB	8	14	11
Sample 727-14 (B-B/A-B)			
ABA	8	8	9
ABB	20	30	17
BBB	38	29	41
AAA	10	4	9
BAA	15	15	17
BAB	9	15	9
Sample 727-16 (B-B/A-B)			
ABA	8	8	9
ABB	19	30	17
BBB	39	27	39
AAA	11	4	9
BAA	14	16	17
BAB	10	15	9
Sample 727-17 ^d (B-B/A-B)			
ABA	11	13	10
ABB	12	25	9
BBB	27	13	31
AAA	35	13	24
BAA	12	25	21
BAB	2	13	4
Sample Rocketdyne (B/A)			
ABA	18	11	...
ABB	24	27	...
BBB	13	17	...
AAA	7	9	...
BAA	20	22	...
BAB	18	14	...

See footnotes at end of table.

TABLE 2. (Contd.)

Polymer	Experimental ^c	Calculated, a, b random	Calculated, a, b triblock
Sample 646-89 (B/A)			
ABA	13	14	...
ABB	18	22	...
BBB	14	9	...
AAA	25	17	...
BAA	22	27	...
BAB	8	11	...
Sample 727-5 (B/A)			
ABA	15	15	...
ABB	14	18	...
BBB	8	5	...
AAA	36	24	...
BAA	20	29	...
BAB	7	9	...
Sample 727-5B (B/A)			
ABA	10	12	...
ABB	17	26	...
BBB	25	14	...
AAA	20	11	...
BAA	20	24	...
BAB	8	13	...
Sample 727-4 (B-A-B)			
ABA	2	14	...
ABB	6	8	...
BBB	16	1	23
AAA	70	46	77
BAA	3	27	...
BAB	3	4	...
Sample 727-7 (B-A-B)			
ABA	2	14	...
ABB	8	10	...
BBB	16	2	26
AAA	61	41	74
BAA	8	28	...
BAB	5	5	...
Sample 727-9 (B-A-B)			
ABA	2	14	...
ABB	11	22	...
BBB	32	9	45
AAA	45	17	55
BAA	5	27	...
BAB	5	11	...

See footnotes at end of table.

TABLE 2. (Contd.)

Polymer	Experimental ^c	Calculated, a,b random	Calculated, a,b triblock
Sample 727-18 (B-A-B)			
ABA	1	15	...
ABB	5	12	...
BBB	23	2	29
AAA	66	36	71
BA ^d	3	29	...
BAB	2	6	...

^a Calculated assuming equal reactivity ratios for random polymers and center blocks.

^b Boldface numbers are the calculated percentages that fall closer to the experimental value.

^c From integrated peak areas of ¹³C NMR quaternary carbon resonances.

^d Center block is a 30% BAMO/70% AMMO random polymer.

CONCLUSIONS AND FUTURE WORK

The analysis of microstructure in oxetane polymers B-A-B and B-(B/A)-B along with several B/A random polymers is easily performed by ¹³C NMR experiments at moderate magnetic field strengths (4.7 tesla). The information obtained from these experiments will help us to understand and/or verify the operative polymerization mechanism. In addition, the combination of this structural analysis with the GPC-LALLS results will allow us to study mechanical properties and adjust synthetic methods to suit our material needs. The block factors and indexes described in this text have been shown to correlate very well with crystallization times measured by FT-IR spectroscopy. We assume that more precise information on block lengths will lead to a better understanding of this important TPE property, and we have begun a study on five B-A-Bs where only the length of the BAMO hard block is varied. Future work will also include a more detailed study of reactivity ratios. We plan to study several B/A random polymers and compare the experimental diad distribution to those predicted by mechanistic models that account for monomer depletion due to differing comonomer reactivity ratios. Finally, we will attempt to do a detailed study of polymer end groups. Our methodology will involve end group functionalization with trifluoroacetyl imidazole and subsequent quantitative ¹⁹F NMR analysis. First, we would like to demonstrate that the polyoxetanes prepared by these methods are largely hydroxy-terminated.

MOLECULAR WEIGHTS, MOLECULAR WEIGHT DISTRIBUTIONS,
AND THERMAL ANALYSIS BY DSC

Mostafa A. H. Talukder, Michael A. S. Hasting,
and Geoffrey A. Lindsay, Investigators

INTRODUCTION

A number of different workers (References 11 through 20) have elaborately described the various aspects of GPC-LALLS technique in terms of its application to the characterization of polymers. Gel permeation chromatography-low angle laser light scattering has proven to be an efficient technique to determine molecular weight (MW) and molecular weight distribution (MWD) of the polymers offering a number of advantages. Gel permeation chromatography-low angle laser light scattering provides very sensitive detection of high MW fractions and is applicable to both linear and branched polymers and their mixtures. Column calibration is eliminated and the sample clarification problems are minimized. The method has been successfully applied to homopolymers. Because the change in refractive index divided by the change of concentration (dn/dc) value is dependent on the composition, problems arise for copolymers if the composition (References 13 and 19) of a copolymer changes with the MW. As a result, the MW and MWD determined for a copolymer may not represent the actual values. However, there is no problem if the composition of polymer is uniform or the dn/dc value of a copolymer solution in a particular solvent do not show any significant change with the MW or the composition.

In this study, the MW and MWD of different oxetane polymers determined by GPC-LALLS using THF as solvent will be discussed in detail. The thermal analysis of the polymers carried out by DSC will be discussed. The physical and thermal properties are essential parameters for determining the ultimate properties of the solid rocket propellants.

THEORETICAL BACKGROUND

Some general equations of the MWs of homopolymers and copolymers in terms of the refractive index increment were derived by Benoit (Reference 13) and other workers (Reference 11 and 12).

For a solution of monodisperse homopolymer, the difference of Rayleigh factor of a polymer solution and that of the solvent at low angle of scattering can be written as

$$R - R_0 = \frac{2\pi^2 \eta_0^2}{N\lambda_0^4} cMv^2 \quad (1)$$

where

- R = Rayleigh factor of polymer solution,
- R₀ = Rayleigh factor of solvent,
- η₀ = Refractive index of the solvent,
- λ₀ = Wavelength of light in vacuo,
- N = Arogadro number,
- c = Concentration of polymer solution,
- v = Refractive index increment of polymer in the particular solvent,
and
- M = Molecular weight of the polymer.

Equation 1 can be written again as

$$R - R_0 = KcMu^2 \quad (2)$$

$$\text{where } K = \frac{2\pi^2\eta_0^2}{N\lambda_0^4}$$

In the case of a polydisperse homopolymer, Equation 2 is written as

$$R - R_0 = Ku^2 \sum C_i M_i \quad (3)$$

where M_i = molecular weight and C_i = concentration of the ith specie (i can be thought of as the degree of polymerization or the number of monomer units in a particular chain). On introducing the average molecular weight, \bar{M} , Equation 3 becomes

$$R - R_0 = Kc\bar{M}u^2 \quad (4)$$

By comparing Equations 3 and 4 \bar{M} can be written as

$$\bar{M} = \frac{\sum C_i M_i}{\sum C_i} \quad (5)$$

which is the weight average molecular weight.

Similarly, under conditions of very dilute solution and low angle, the difference between the Rayleigh factor of the solution of copolymer (polydisperse with respect to molecular weight and composition) and that of the solvent can be expressed as

$$R - R_0 = K \sum C_i M_i v_i^2 \quad (6)$$

The apparent molecular weight, M*, of the copolymer can be introduced as

$$R - R_0 = KcM^*v^2 \quad (7)$$

where v = refractive index increment of the copolymer solution.

By comparing Equations 6 and 7, M^* can be written as

$$M^* = \frac{1}{cv^2} \cdot \sum c_i M_i v_i^2 \quad (8)$$

or

$$M^* = \frac{1}{v^2} \sum \gamma_i M_i v_i^2 \quad (9)$$

$$\text{where } \gamma_i = \frac{C_i}{\sum C_i} .$$

i.e., γ_i is the relative concentration of the molecules of composition W_i . It is important to note from Equations 4, 5, and 8 (or 9) that for homopolymers the molecular weight is independent of the refractive index increment of the polymer, whereas for copolymers the molecular weight can depend on the refractive index increment of the copolymer if composition varies with molecular weight. The refractive index of the solvent used must be chosen with care (Reference 13).

On the basis of the additivity of polarizabilities (References 11 and 13), the refractive index increment of a copolymer, especially a block copolymer, formed of monomer A and monomer B can be written as

$$v = Wv_A + (1 - W)v_B \quad (10)$$

where

- v_A = Refractive index increment of homopolymer A,
- v_B = Refractive index increment of homopolymer B, and
- W = Weight fraction of component A.

It should be noted that the refractive index increment of the copolymer may be positive, negative, or zero for the signs v_A and v_B depend on the solvent used. On substitution of v according to Equation 10, Equation 9 can be expressed as

$$M^* = \frac{1}{v^2} \sum u_i M_i (W_i^2 v_A^2 + (1 - W_i)^2 v_B^2 + 2 W_i (1 - W_i) v_A v_B) \quad (11)$$

on introducing the weight average molecular weight of component A (Equation 12) and component B (Equation 13)

$$\bar{M}_w^A = \frac{1}{W} \sum \gamma_i M_i W_i^2 \quad (12)$$

$$\bar{M}_w^B = \frac{1}{(1-W)} \sum \gamma_i M_i (1-W_i)^2 \quad (13)$$

in Equation 11, M^* becomes

$$M^* = \frac{1}{v^2} (W \bar{M}_w^A v_A^2 + (1-W) \bar{M}_w^B v_B^2 + 2 v_A v_B \bar{M}_w^{AB}) \quad (14)$$

where

$$\bar{M}_w^{AB} = \sum \gamma_i M_i W_i (1-W_i) \quad (15)$$

On rearrangement, \bar{M}_w^{AB} can be expressed as functions of \bar{M}_w^A , \bar{M}_w^B , and \bar{M}_w as follows

$$\bar{M}_w^{AB} = \frac{1}{2} \sum \gamma_i M_i (1-W_i^2 - (1-W_i)^2) \quad (16)$$

$$\frac{1}{2} (\bar{M}_w - W \bar{M}_w^A - (1-W) \bar{M}_w^B) \quad (17)$$

Substituting the value of \bar{M}_w^{AB} (equation 17) in equation 14, M^* is written as

$$M^* = \frac{1}{v^2} (W \bar{M}_w^A v_A^2 + (1-W) \bar{M}_w^B v_B^2 + 2 v_A v_B \cdot \frac{1}{2} (\bar{M}_w - W \bar{M}_w^A - (1-W) \bar{M}_w^B)) \quad (18)$$

or

$$M^* = \frac{1}{v^2} (\bar{M}_w v_A v_B + W \bar{M}_w^A v_A (v_A - v_B) + (1-W) \bar{M}_w^B v_B (v_B - v_A)) \quad (19)$$

It is noteworthy that if v does not depend on any particular species (i.e., $v_A = v_B$), the apparent molecular weight M^* is equal to \bar{M}_w . Obviously, if v is zero, M^* goes to infinity. In the overall theoretical discussion, we have shown that the MW of a homopolymer is independent of the refractive index increment while that of a copolymer can depend on the refractive index increment and thus can vary with the solvent used. We have also shown that the refractive index increment of polymer does not depend on the MW but depends on the composition of the polymer. Furthermore, if the refractive

index increment of a copolymer does not depend on any particular species, the apparent MW is equal to the weight average molecular weight.

RESULTS

The dn/dc value of polymers in THF solution is directly proportional to the concentration (Figure 16). The dependence of dn/dc values of oxetane polymers versus the molecular weight is shown in Figure 17. Although the experimental data are scattered, the dn/dc values did not show any significant change. Similarly, on the other hand, the dn/dc values of oxetane polymers, as expected, varied with the composition of polymers (Figure 18). The dn/dc values increased with the BAMO content of the polymers.

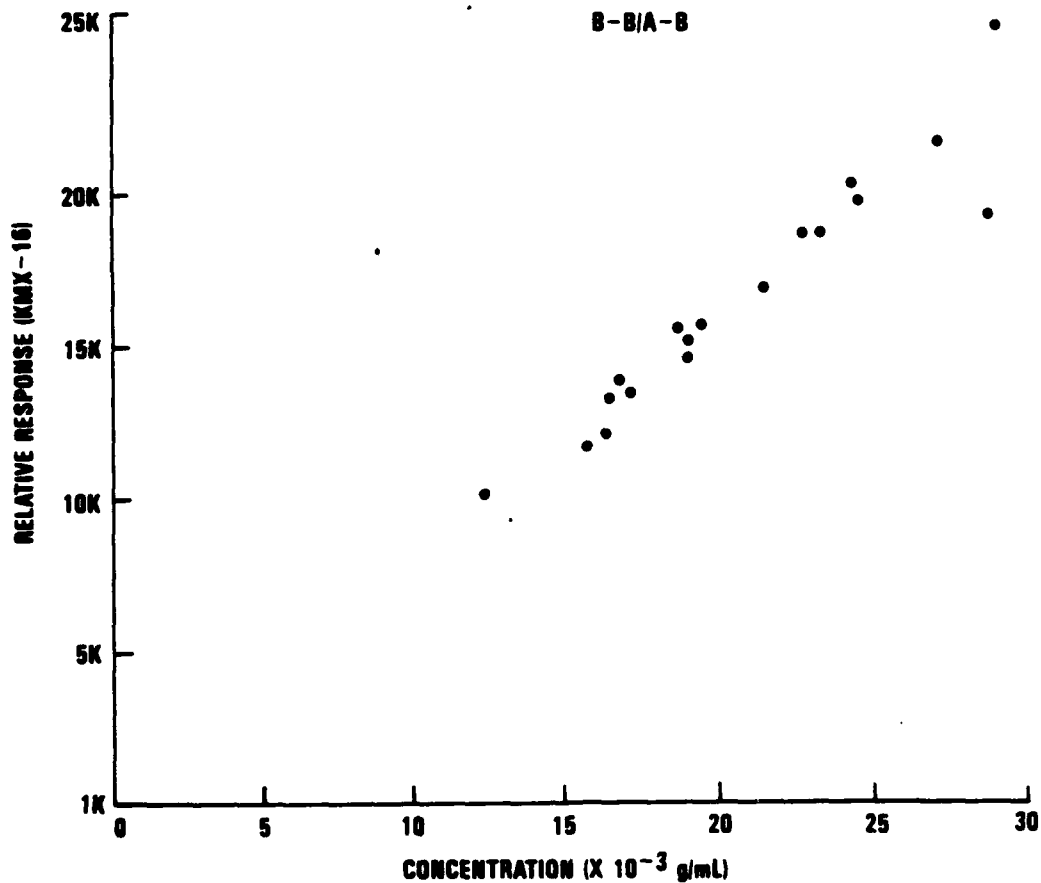


FIGURE 16. Relative Response (KMX-16) of Oxetane Polymers in THF Versus Concentration of Polymers.

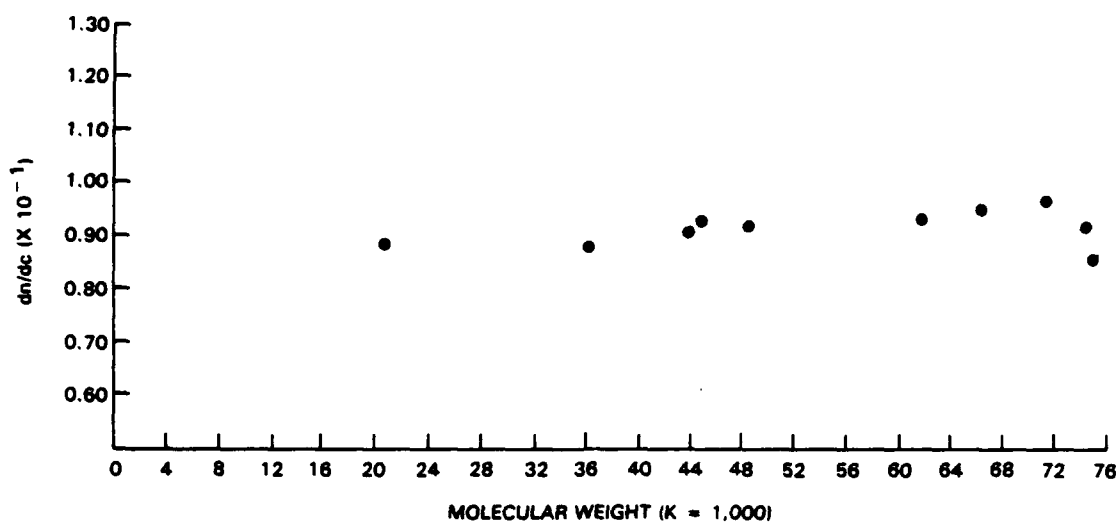


FIGURE 17. dn/dc of Oxetane Polymers in THF Versus MW of Polymer.

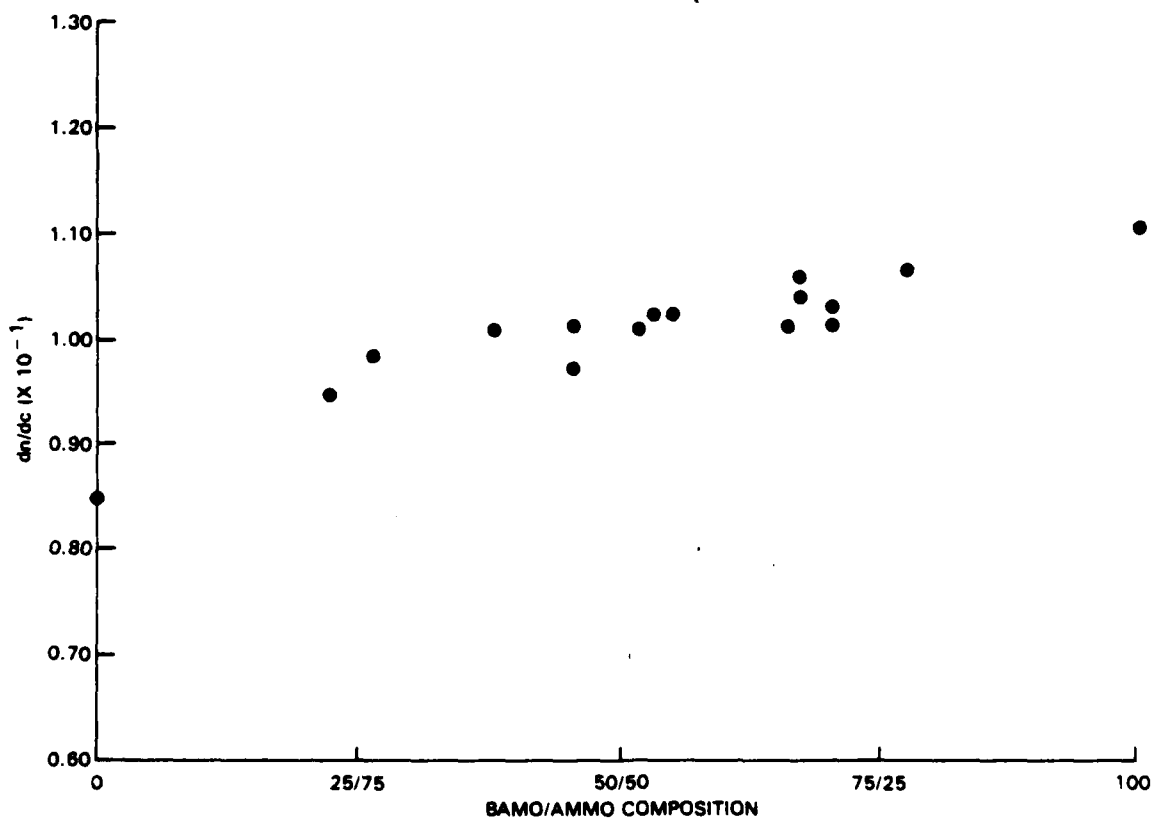


FIGURE 18. dn/dc of Oxetane Polymers in THF Versus Composition of Polymers.

EXPERIMENTAL SECTION

Materials

Oxetane polymers of BAMO and NMMO were prepared in the laboratory at NWC and oxetane polymers of AMMO and BAMO were prepared at Aerojet. In both cases, the polymers were prepared using a special difunctional cationic initiator, p-dicumyl chloride, in combination with AgSbF_6 .

Procedure

GPC-LALLS. All measurements of MW and MWD determinations were made in THF at room temperature. The dn/dc determination samples were prepared in concentrations ranging between 3 to 10 mg/ms. Specific refractive index increment values were measured at 6328 \AA with a Chromatix KMX-16 laser differential refractometer. Gel permeation chromatography-low angle laser light scattering measurements were made at 100, 500, 1000, and 10,000 \AA with the eluant flow rate at 0.75 mL/min. The eluant from the columns was passed through the cell of a Chromatix KMX-6 LALLS unit and then pressed through a differential refractive index (DRI) detector. Sample preparation for GPC measurements was the same as dn/dc analysis. An injection volume of 100 microliters was used to obtain a good signal for the LALLS detector. The LALLS was employed with an angle of 6 to 7 degrees and a 0.2 millimeter field stop to minimize background noise. The composition of the oxetane polymers were determined by FT-NMR and FT-IR analyses. The schematic diagram of GPC-LALLS is shown in Figure 19.

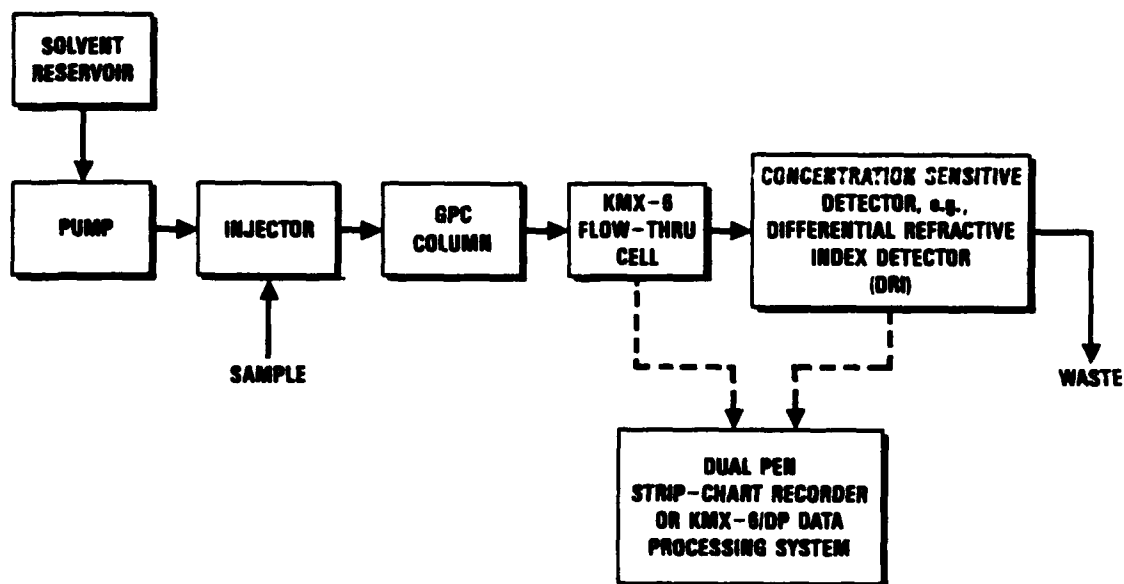


FIGURE 19. Schematic of GPC-LALLS System.

Thermal Analysis. Samples were initially heated to 100°C and then cooled to room temperature. The heat-treated samples were analyzed for glass transition temperature (T_g) and melting temperature (T_m) at a heating rate of 10°C/min.

RESULTS AND DISCUSSION

GPC-LALLS

Table 3 shows the experimental data of oxetane polymers including polystyrene standards. The experimental data mainly represent the MW and MWD values of two series of polymers such as BAMO-NMMO copolymers and AMMO-BAMO copolymers. The MW (\bar{M}_n) range varies from 16 000 to 223 000. The MWD is approximately 1.5 which indicates the narrow

TABLE 3. Molecular Weight and Molecular Weight Distribution of Oxetane Polymers by GPC-LALLS.

Sample	Polymer ^a	\bar{M}_w , K	\bar{M}_n , K	\bar{M}_w/\bar{M}_n
1196-06	B-N-B	24.0	16.0	1.5
1196-09	B-N-B	270.0	223.0	1.2
646-8	A	17.4	14.7	1.2
795-72	B	22.1	8.4	2.6
727-5B	B/A	63.2	53.7	1.2
727-5	B/A	44.3	38.6	1.2
646-89	B/A	22.8	9.1	2.5
727-4	B-A-B	75.3	61.1	1.2
727-9	B-A-B	44.8	38.3	1.2
727-7	B-A-B	35.8	22.6	1.6
646-91A	B-B/A-B	591.4	167.0	3.5
646-79B	B-B/A-B	231.7	84.1	2.8
727-2	B-B/A-B	127.3	86.2	1.5
646-94	B-B/A-B	94.2	71.8	1.3
646-99	B-B/A-B	67.0	57.1	1.2
727-10	B-B/A-B	56.8	33.2	1.7
727-11	B-B/A-B	48.2	32.9	1.5
Polystyrene (STD-51000)		50.3 (51.0) ^b	46.3	1.08 (1.06)
Polystyrene (STD-35000)		35.1 (35.0)	33.6	1.04 (1.06)

^a A = AMMO, B = BAMO, N = NMMO.

^b Actual value = ().

NWC TP 6945

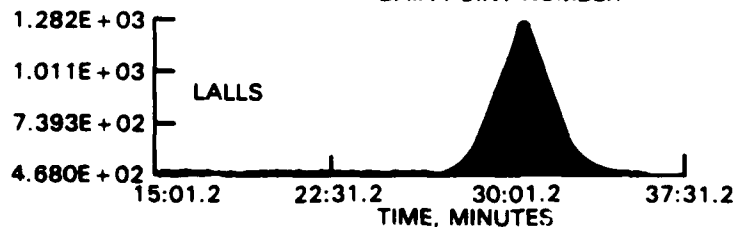
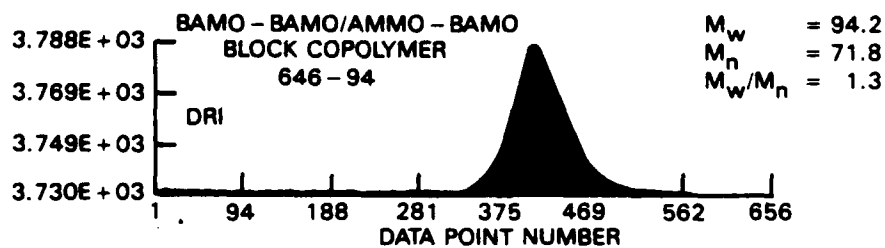
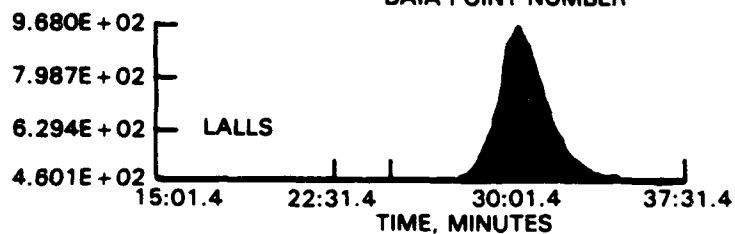
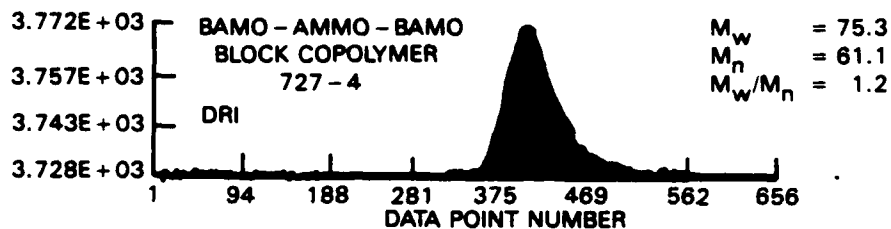
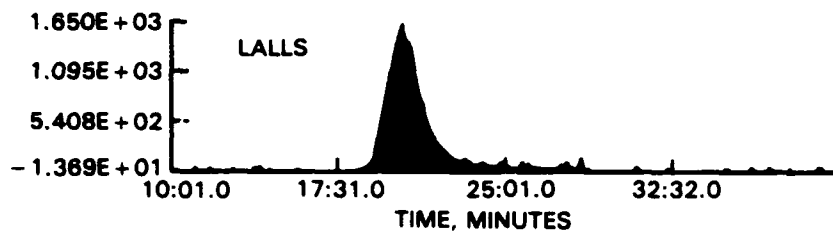
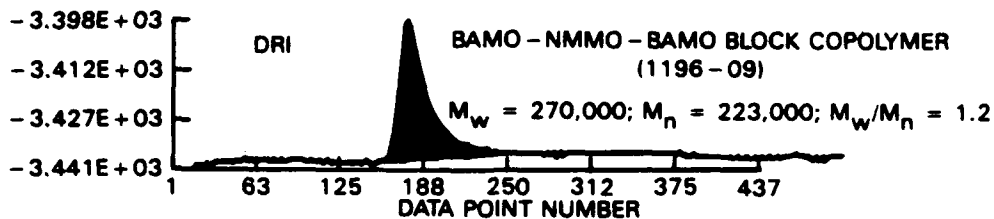


FIGURE 20. GPC-LALLS Chromatograms of Oxetane Polymers.

distribution of molecular weights. We have also shown that for polystyrene standards the values of MW and MWD were in good agreement with the values reported by the manufacturing company. Table 4 gives the values of MW and MWD of oxetane polymers determined by GPC-LALLS as well as conventional GPC (using polystyrene standards). The results are interestingly close. The GPC-LALLS chromatograms of oxetane polymers are shown in Figure 20. The symmetrical curves indicate the narrow MWD of polymers.

TABLE 4. Molecular Weight and Molecular Weight Distribution of Oxetane Polymers.

Sample	Polymer	GPC-LALLS			GPC ^a		
		\bar{M}_w , k	\bar{M}_n , k	\bar{M}_w/\bar{M}_n	\bar{M}_w , k	\bar{M}_n , k	\bar{M}_w/\bar{M}_n
1196-06	B-N-B	24.0	16.0	1.5
1196-09	B-N-B	270.0	223.0	1.2
727-3	B-B/A-B	73.8	60.5	1.2	60.4	45.6	1.3
727-4	B-A-B	75.3	61.1	1.2	93.6	69.0	1.4
724-5	B/A	44.3	38.6	1.1	48.3	34.5	1.4
727-7	B-A-B	35.6	22.7	1.6	36.1	22.0	1.6
727-8	A	17.4	14.7	1.2	15.6	12.6	1.3
727-9	B-A-B	44.8	38.3	1.2	39.4	30.0	1.3
727-10	B-B/A-B	56.8	33.2	1.7	41.9	25.1	1.7
727-11	B-B/A-B	48.2	32.9	1.5	36.6	23.8	1.5

^a Data obtained with polystyrene standards.

Thermal Analysis

The DSC curves of homopolymers and copolymers were shown in Figures 21 through 23. PolyBAMO has a sharp melting point at about 92°C (Figure 21). Because the amorphous region formed during quenching of the polymer, a T_g was observed at about 22.8°C. PolyAMMO and polyNMMO have only T_g and no melting points as expected. The T_g of polyAMMO was found to be lower than that of polyNMMO, probably due to the difference in the side groups. The side group (-CH₂ONO₂) is more bulky than the -CH₂N₃ group of polyAMMO. The block copolymers of BAMO with AMMO or NMMO (Figures 2 through 24) exhibit a well-defined two-phase domain structure which indicated the crystalline and soft blocks of the polymers. The broadness of melting point (Figures 22 and 23) at the onset temperature region may be due to the diffused imperfect BAMO-AMMO block end. The experimental data are summarized in Table 5. The T_g and T_m of polymers prepared by varying composition range from -22 to -43°C, and 58 to 92°C, respectively. The wide range of variation of T_g and T_m indicate that the polymers can be easily tailored to fit the end product need. Although there is no direct relationship between the T_g and chain length of the polymers, T_m seems to vary with the MW of polymers as shown for samples 727-4, 727-9, and 727-7 B-A-B block

copolymers. The variation may be because of the variation of crystalline BAMO block length.

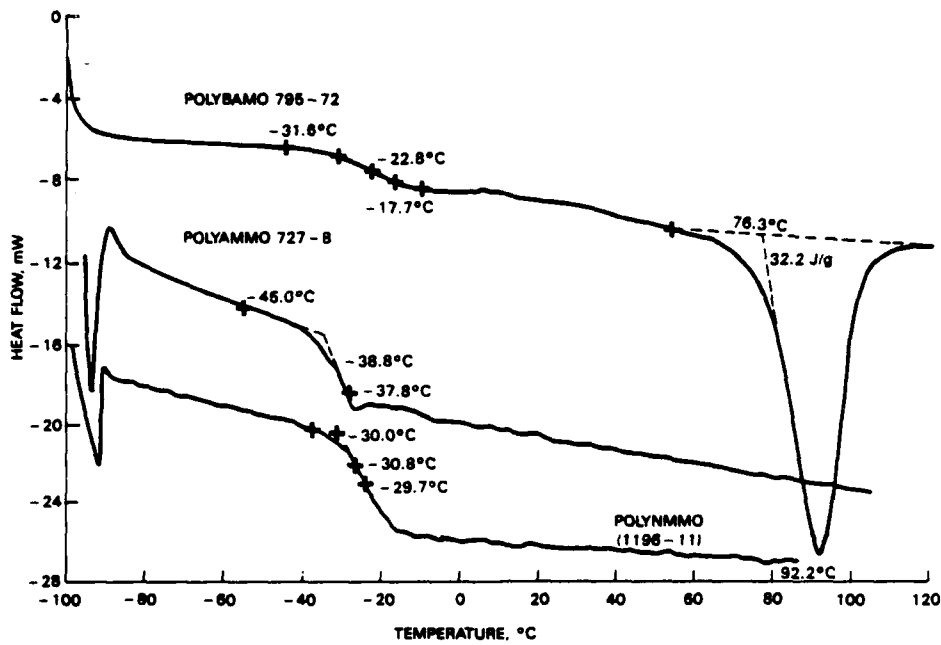


FIGURE 21. DSC Thermograms of Oxetane Homopolymers.

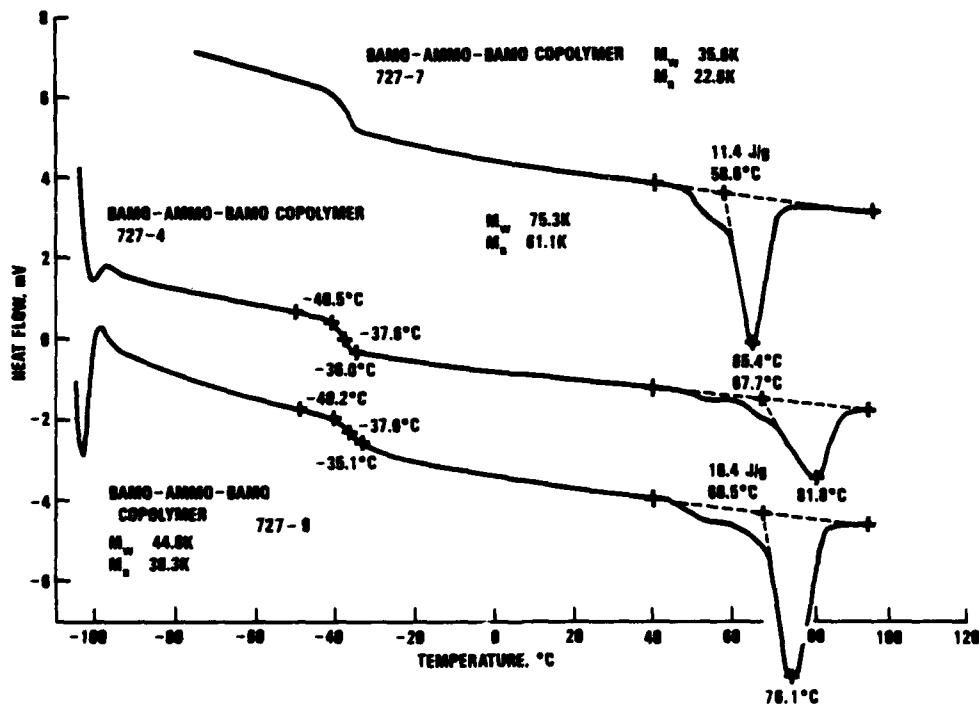


FIGURE 22. DSC Thermograms of BAMO-AMMO-BAMO Copolymers.

NWC TP 6945

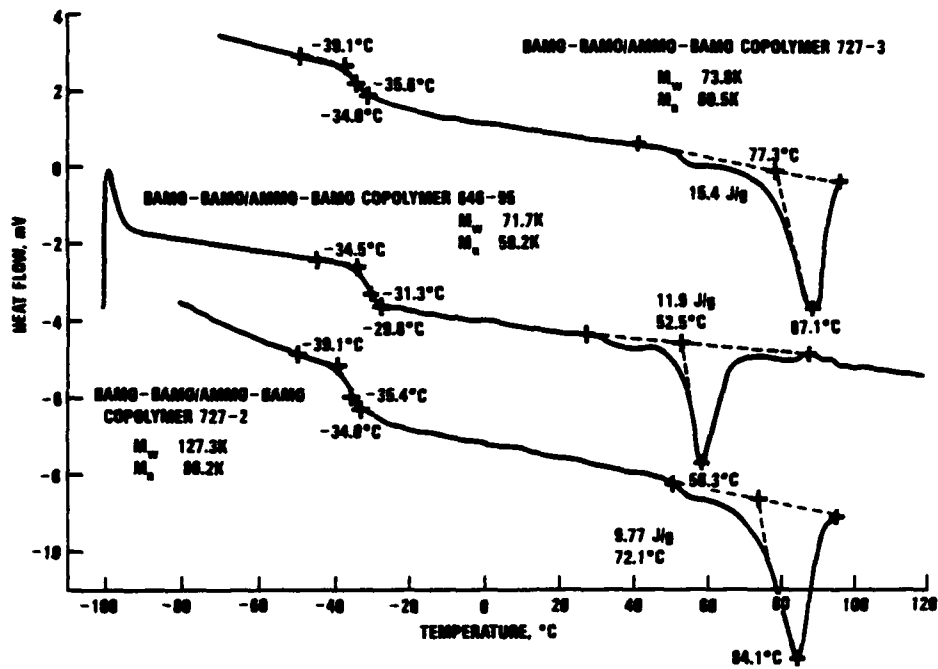


FIGURE 23. DSC Thermograms of BAMO-BAMO/AMMO-BAMO Copolymers.

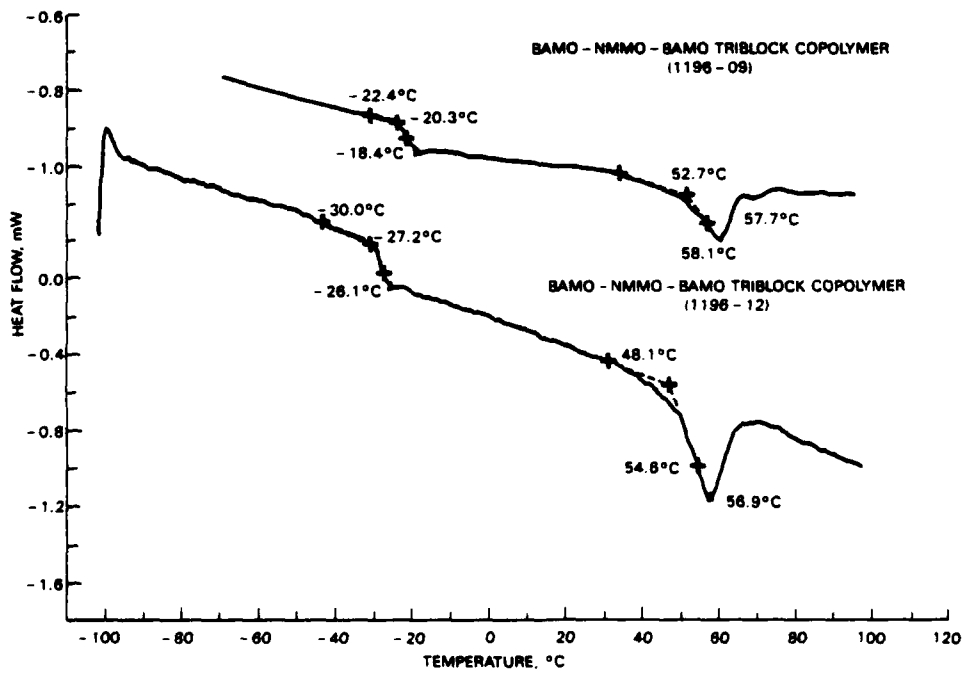


FIGURE 24. DSC Thermograms of BAMO-NMMO-BAMO Copolymers.

TABLE 5. Thermal Analysis of Oxetane Polymers.
DSC Data: Rate is 10°C/min.

Sample	Polymer	T _g , °C	T _m , °C	ΔH, J/g	\bar{M}_w , K	\bar{M}_n , K	\bar{M}_w/\bar{M}_n
795-72	B	-22.8	92.2	32.2	22.1	8.4	2.6
727-8	A	-38.8	17.4	14.9	1.2
727-5B	B/A	-34.3	78.3	8.3	63.2	53.7	1.1
646-89	B/A	-43.5	22.8	9.1	2.5
727-4	B-A-B	-37.6	81.8	9.48	75.3	61.1	1.2
727-9	B-A-B	-37.0	76.1	16.4	44.8	38.3	1.2
727-7	B-A-B	-36.3	65.4	11.4	35.6	22.6	1.6
646-91A	B-B/A-B	-36.1	83.5	22.8	591.4	167.0	3.5
646-79B	B-B/A-B	-32.5	85.7	16.1	231.7	84.1	2.8
727-2	B-B/A-B	-35.4	84.1	9.7	127.3	86.2	1.5
727-3	B-B/A-B	-35.6	87.1	15.4	73.8	60.5	1.2
646-95	B-B/A-B	-31.3	58.3	11.9	71.7	59.2	1.2
1196-11	N	-30.8
1196-12	B-N-B	-27.2	56.9
1196-09	B-N-B	-20.3	58.1	...	270.0	223.0	1.2

CONCLUSIONS

Polyoxetanes made at -95°C with the dicarbocationic initiator, p-dicumyl hexafluoroantimonate, were analyzed for MW and thermal transitions. The MWD were characterized by GPC-LALLS-DRI and found to be fairly narrow indicating a quasi-living polymerization mechanism. Molecular weights increased as the monomer to initiator ratio was increased. However, the number of moles of polymer chains produced per mole of initiator is 40 to 60% less than expected. This may indicate a side reaction is consuming some of the initiator. Thermal transitions were characterized by DSC. Glass transition temperatures were typically -35°C, and crystalline melting points ranged from 60 to 85°C depending on composition and blocklength.

UTILITY OF THERMAL AND STRUCTURAL INFORMATION

Rena Y. Yee, Investigator

INTRODUCTION

The polymer structures characterized include poly(BAMO)-(Bn), poly(AMMO)-(An), a random copolymer of the above two monomers-(B/A) and block copolymer-(B-(B/A)-B). The BAMO content in the central block of block polymers is 0, 30, and 50%.

This section will show how some thermal and mechanical properties of these copolymers are related to their microstructures, which have been shown in the previous sections. The mechanical properties are obtained from uniaxial tensile testing.

EXPERIMENTAL SECTION

Except for the mechanical properties and morphological observations, all of the data discussed here are taken from the previous sections. The tensile mechanical tests were performed in an Instron Universal Testing Instrument, model 1122, Instron Corporation, Canton, Mass. The specimens (1 by 5 by 30 mm) were prepared by compression molding. The small specimen size was chosen because more materials are available only in small quantities. The rate of cross head movement in the Instron is 5 mm/min. The morphological observations were made under a Carl Zeiss polarizing microscope.

DISCUSSION

Glass Transition Temperature

The glass transition temperature (T_g) of some of the oxetane polymers are given in Table 6. The T_g of poly(AMMO)-(An) is -39°C . Poly(BAMO)-(Bn), sample 795-72, shows a very weak transition around -23°C . Since it is very weak compared with the poly(AMMO) transition, the poly(AMMO) T_g will be used as reference. The difference between the T_g of each sample and T_g of the poly(AMMO) is listed as ΔT_g .

The T_g generally involves motion of short chain segments in the amorphous region. This is more a local phenomenon. The B-A-B type block polymers' center block contains the poly(AMMO) structure. They are not expected to show much change in T_g from that of An. Their ΔT_g in Table 6 are indeed small.

TABLE 6. Glass Transition.

Sample	Type	-BBB-, %	T _g	ΔT _g
646-79B	B-(B/A)-B	44	-32	7
646-91A	B-(B/A)-B	53	-36	3
646-95	B-(B/A)-B	35	-31	8
727-2	B-(B/A)-B	34	-35	4
727-3	B-(B/A)-B	38	-36	3
727-4	B-A-B	15	-38	1
727-7	B-A-B	16	-36	3
727-9	B-A-B	32	-37	2
727-20C	B-A-B	30	-36	3
727-5B	B/A	25	-34	5
646-89	B/A	14	-43	-2
795-72	B _n	100	-23	...
727-8	A _n	0	-39	0

The BAMO end block of the B-(B/A)-B copolymers can be assumed to be not influencing. Therefore, the T_g is expected to be similar to that of a B/A random copolymer. The effect of BAMO on T_g can be treated either as a diluent of AMMO or a component in a mixture with AMMO. Gordon and Taylor gave an equation for T_g of random copolymer (Reference 21):

$$(T_g - T_{g,a}) W_1 + K (T_g - T_{g,b}) W_2 = 0 \quad (20)$$

where

- w₁ and w₂ = weight fractions of monomer a and b,
- T_{g,a} and T_{g,b} = T_g of the homopolymers,
- T_g = the T_g of the copolymer, and
- K = a constant proportional to the thermal expansion coefficient.

If the K term is constant, this equation would be just the rule of mixture. The T_g of a 50% BAMO would be midway between -39 and -23°C (therefore, ΔT_g would be -8°C). The observed ΔT_g are 7, 3, and 8. The agreement is close. There is no explanation on the smaller ΔT_g for sample 646-91A. According to the rule of mixture, the copolymer containing 30% BAMO would show a T_g around 4.8°C. The observed values are 3, 4, and 5. No variation of ΔT_g with MW has been observed in these samples. The variation of T_g of polystyrene with MW has been shown by Fedors (Reference 22). The rate of change is very small beyond the MW of 10,000. Possibly, the MW of AMMO sequence in these polymers are also beyond the rapid changing range. This point will be clarified when more data are available.

In summary, the BAMO end blocks do not seem to interfere with the T_g of the center AMMO block. The presence of BAMO in the close vicinity of the

AMMO modifies it according to the rule of mixture. There are some minor fluctuations which are probably due to other differences in microstructures.

Melting Temperature

The melting behaviors of TPEs are very important in processing. If the melting temperature is too high, the high processing temperature would affect other ingredients in the formulations. If the temperature is too low, the material would undergo transition too easily (e.g., storage in tropical weather). Nahlovsky recommended sharp melting in the selected temperature range (Reference 23). The careful and specific microstructure analysis performed on this series of samples make them very good candidates for exploring the structure-property aspect in melting behavior. This information can be used to help design the desirable melting temperature to synthesize copolymers be.

In this series of copolymers, the BAMO sequence is crystalline and the AMMO sequence does not crystallize. Therefore, the melting behavior is associated with the BAMO sequence. The amorphous material can be present inside the crystalline domain and thus modify the melting either in terms of melting temperature or heat of melting. Because it involves the melting of long crystalline polymer chains, the melting behavior is more a global phenomenon as compared to the local one in T_g . Therefore, the structures of both the hard and soft blocks have to be considered in the treatment of melting of block copolymers.

A theoretical treatment of the equilibrium crystallization of random copolymers has been developed by Flory (References 24 and 25). The presence of the AMMO unit that cannot be crystallized can be treated as an interference to the crystallization process. The melting requirement depends on how perfect the crystalline material has been prepared. The melting temperature can be expressed in the following equation

$$\frac{1}{T_m} - \frac{1}{T_m^0} = (-RLnX_B) / \Delta H_v \quad (21)$$

where

- T_m^0 = the melting temperature of an infinitely long crystal of homopolymer B,
- ΔH_v = the enthalpy increase on melting a mole of B, and
- X_B = the mole fraction of B.

In order to consider the sequence distribution in the copolymers, the mole fraction " X_B " term should be replaced by a sequence propagation probability term. This is similar to the melting point depression expression. The equation can be rearranged to give

$$\frac{\Delta T_m}{T_m} = (-RT_m^0/\Delta H_v) \cdot \ln X_B \quad (22)$$

Plotting $\Delta T_m/T_m$ against $\ln X_B$ should have a slope of $(-RT_m^0/H_v)$. The next factor to be considered is which expression should be used for the X_B term? There are four choices: total BAMO content of the copolymer; BAMO triad content (page 20); block factor (PAGE 20); and the ratio of the BAMO end block to the length of the whole triblock. Total BAMO content of the copolymer does not distinguish the different types of BAMO in the triblock. The ratio of the BAMO end block to the length of the whole triblock is not used because the number is not known for all of the polymer samples. The results of using the percent -BBB- and block factor are shown in Figure 25. Except for sample 646-95, the points do generally scatter around a line.

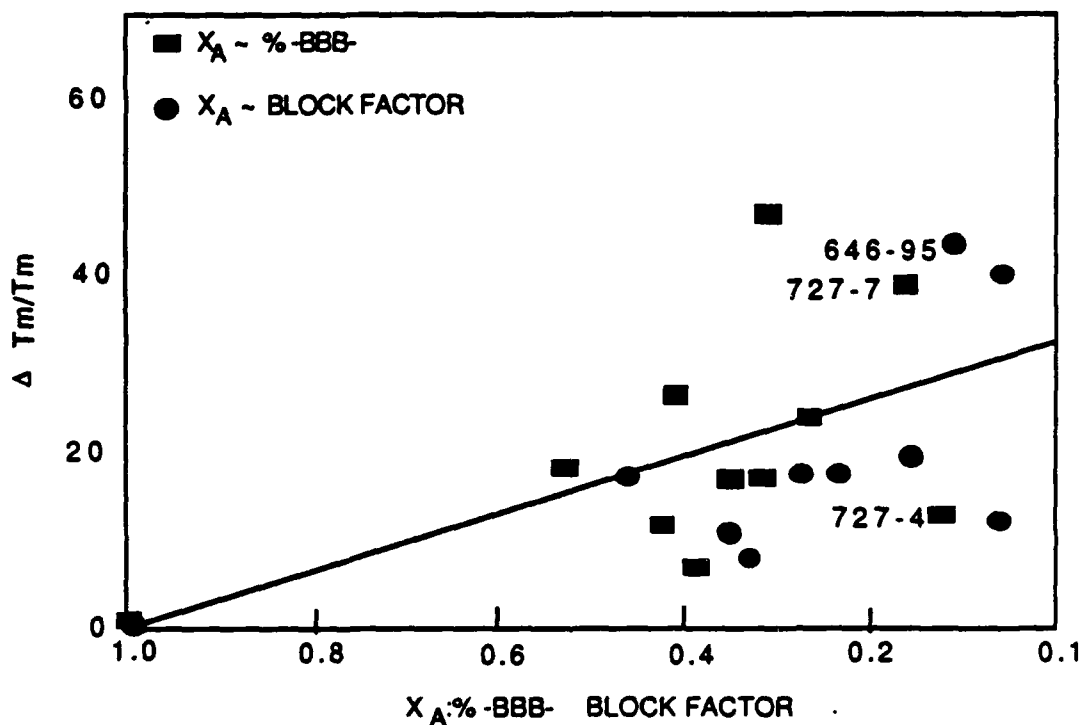


FIGURE 25. Structure and Melting Temperature.

Because of the scattering of data points, an improved model is needed. The samples 727-4 and 727-7 show more deviation than the other samples. They are both of B-A-B structure. This is different from the random copolymer structure. Flory predicted that the melting point depression of block copolymer is still a function of the sequence length of the crystalline monomer. However, the effect is not as great as for a random copolymer of the same composition. The samples in our series can be separated into four types:

Bn: homopolymer of the crystalline monomer.

B/A: This structure can be treated as the random distribution of the AMMO among the BAMO controlled by probability. According to Flory's model, there can be crystallinity in the B/A samples. Both our NMR and FT-IR support this idea. The NMR results indicate more percent -BBB- in the samples than expected in the BAMO end blocks. Fourier transform infrared shows that the two B/A copolymers do crystallize even though their crystallization half life ($t_{1/2}$) are much longer than the other block copolymers. The melting peak is probably so small that it is not noticed in the DSC curves.

B-A-B: The crystalline BAMO end block modified by the presence of the AMMO in the center block. The effect is less than that of B/A copolymers.

B-(B/A)-B: These polymers contain the features of both the Bn and B/A structures.

The DSC curves of Figures 21 through 24 confirm this general observation. The poly(BAMO) has a sharp melting peak with very high heat of melting. All the other melting peaks have a broad shoulder on the lower temperature side. Some of them may be considered as overlapping separate peaks.

It should be emphasized that this exercise is only an exploratory study to begin accumulating baseline information of structure-property relationships. After a set of target properties of the copolymer has been chosen, the information can be used to help design the structures of candidates to be synthesized. The number of samples is not sufficient to cover such a large variation in structures. The DSC results are definitely far from the ideal equilibrium melting and crystallization investigation (Reference 26). A series of more well controlled less varying block copolymers is being designed to elucidate the structural affects.

Heat of Melting

The heat of melting of these copolymers is reported in Table 7. The melting is from the BAMO sequence. The ratio of BAMO/AMMO varies. In order to account for these facts, the heat of melting values are normalized with percent -BBB- and block factor; the results are shown in the last two columns. The general trend observed is that the normalized heat of melting of the B-A-B copolymers are higher than the other copolymers. The BAMO triads in the B-A-B polymers are all in the BAMO end blocks. They are probably of higher sequence lengths than those found in the center (B/A) block. Therefore, it is reasonable that their heat of melting is higher. We cannot explain why the normalized heat of melting of the poly(BAMO) is lower. One possible cause is that this BAMO sample is of much lower molecular weight than the other copolymers in this series (8.5 K).

TABLE 7. Heat of Melting.

Sample	Type	-BBB-, %	ΔH_m (J/g)	$\Delta H_m /$ -BBB-, %	$\Delta H_m /$ Block factor
646-79B	B-(B/A)-B	44	16.0	23	46
646-91A	B-(B/A)-B	53	23.0	43	49
646-95	B-(B/A)-B	35	12.0	34	60
727-2	B-(B/A)-B	34	9.8	29	35
727-3	B-(B/A)-B	38	15.4	40	45
727-4	B-A-B	15	9.5	63	73
727-7	B-A-B	16	11.4	71	95
727-9	B-A-B	32	16.0	50	61
727-20C	B-A-B	30	9.8	33	33
727-5B	B/A	25	8.3	33	49
795-72	Bn	100	32.0	32	32

CRYSTALLIZATION FROM THE MELT

Each sample was melted on a cleaned microscope slide with a cover glass on a hot plate then removed from the hot plate to room temperature for crystallization. The morphology was observed under a Carl Zeiss polarizing microscope equipped with a rotating stage. Photomicrographs were taken periodically until the spherulites filled the sample space. The time required varied from one minute to more than 20 hours. The average spherulite size was determined from the photomicrographs. The crystal birefringence was used to determine the sharpness of the crystal which was related to the regularity of the crystal chain folding. For comparison purposes, the sample size, temperature of melting, and all other handling procedures were kept as consistent as possible. The control is not as good as observation in a hot stage.

RESULTS AND DISCUSSION

As mentioned in the experimental section, the control in performing this set of experiments was not vigorous. The morphology observation was more qualitative than quantitative. The samples were used without further purification. Whenever unusual features were presented (e.g., high concentration of catalyst left in the sample), it would show up in the different degree of nucleation in the spherulitical growth. Our observation assumed that the sample purity was comparable from sample to sample.

Given the above limitations, the type of observation can provide information on how easy the melt recrystallizes and what type of morphology is obtained. We also were able to observe any unusual features in the melting behavior. For instance, samples 727-4 and 727-8 showed a tendency for strain-induced crystallization with very high orientation in the strain direction. Sample 727-18 was degraded easily by heat while other samples showed no sign

of degradation. All the samples crystallized from melt showed spherulitic crystal growth except for the strain induced crystallization. The results are summarized in Table 8.

TABLE 8. Morphology Observations.

Sample	Spherulite size, μ	Remarks
646-79B	30	Medium sharpness
646-91A	2	Sharp and fast
646-91B	5	Sharp and fast
646-95	10	Fast
646-98	10-20	...
646-99	10-20	...
727-2	300	Very diffuse, fast
727-3	30	Medium sharpness
727-4	30-50	Diffuse crystalline
727-7	10	Very sharp and fast
727-9	30-50	Medium sharpness

The regularity of the crystal chain folding could be observed by comparing the sharpness of the Maltese cross in the extinction pattern of the spherulites under polarized light. The higher the regularity in the crystalline chain folding, the sharper the extinction pattern, the higher the birefringence. More details will be discussed in relationship with the microstructures later.

The morphology of recrystallization from solution through evaporation were observed for two samples. These trends were also spherulitic but the spherulite size was smaller than 5 micrometers. The time for crystallization from the melt was slower than the same sample from the solution.

Comparison of Different Types of Copolymers

The general trends of glass transition and melting associated with structures have been briefly discussed. They will be used to compare polymers of different structures. The various micro-structures and properties of six polymers are listed in Table 9. Most of the parameters have been used before. The end block BAMO sequence length is calculated from the H-S-H molar composition given in Table 1. The block size and ratio of center to end blocks are important factors in the melting behavior and mechanical properties of these copolymers.

TABLE 9. Microstructures and Properties.

Properties	Samples					
	646-79B	727-2	727-3	727-4	727-7	727-9
\bar{M}_n , K	81	84	61	60	23	38
\bar{M}_w/\bar{M}_n	2.8	1.5	1.2	1.2	1.6	1.2
Structure	B-(B/A)-B	B-(B/A)-B	B-(B/A)-B	B-A-B	B-A-B	B-A-B
% BAMO in center block	50	30	30	0	0	0
B/A	69/31	53/47	51/49	23/77	26/74	45/55
End block BAMO, K	17	9	3	8
% -BBB-	44	34	38	15	16	32
Block factor	35	28	34	13	12	26
ΔT_g ($T_g - T_{g, A_n}$)	7	4	3	1	3	2
ΔT_m ($T_m - T_{m, B_n}$)	-6	-8	-5	-10	-27	-16
ΔH_m , J/g	16	9.8	15.4	9.5	11.4	16
ΔH_m (Block factor)	46	35	45	73	95	61
$t_{1/2}$ (Recrystallization half life turn, min)	1.5	3	1	85	33	45
Spherulite, μ	30	300	30	30-50	10	35-50
Sharpness of crystal	medium	very diffuse	medium	diffuse	sharp	medium
Modulus, psi	565	169
Maximum stress, psi	214	158
Strain at maximum stress, $\Delta l/l_0$	0.26	0.51
Strain at failure, $\Delta l/l_0$	0.42	0.72

Comparison of B-A-B Polymers (Samples 727-4 Versus Sample 727-7)

The MWs of samples 727-4 and 727-7 are different but the ratios of end block to the center block are similar. Their percent -BBB- and block factors are also similar. The sample 727-4 has an end block about three times of that of sample 727-7. The affect of size difference is usually more prominent in the lower molecular weight cases. This results in a larger melting temperature depression for sample 727-7. The reverse is observed for other properties. The sample 727-7 shows higher heat of melting (both original and normalized). Its $t_{1/2}$ is shorter. The shorter the crystallization time, the easier the sample crystallizes. This indicates that the crystallinity is higher in sample 727-7 despite its lower molecular weight. The spherulites observed in sample 727-7 are generally smaller but sharper. The DSC melting peak of sample 727-7 is also sharper. These indicate that sample 727-7 has a lower molecular weight but has a higher order of BAMO sequence.

Comparison of B-(B/A)-B (Sample 727-2 Versus Sample 727-3)

The sample 727-3 has lower dispersity in MW, higher percent -BBB- and block factor. These signal the better BAMO sequence order despite smaller molecular weight. It also results in shorter crystallization time and sharper spherulites as is the case of sample 727-7. The melting temperature depression of sample 727-3, however, is smaller than sample 727-2. This observation is opposite that of sample 727-7. The BAMO end block sequence length is much higher for sample 727-3. Though there is not enough data to draw a conclusion, there is a big temptation to say that the MW effect has been levelled off in this pair of samples.

Comparison of Different Amounts of BAMO In Center Block (Sample 646-79B Versus Sample 727-2)

Their MWs are comparable. The sample 646-79B contains 50% BAMO in the center block while sample 727-2 has only 30%. The sample 646-79B contains more BAMO, the BAMO block factor is higher. These result in less melting temperature depression, higher heat of melting, faster crystallization and sharper spherulites. Because of the higher BAMO content in the center block, the change in T_g is also higher than sample 727-2. These facts also reflect in higher modulus and maximum stress but sample 646-79B is lower in elongation in tensile testing. Aeroject indicates that these moduli are too high for neat binder. They would like to prepare the polymers with lower modulus and higher elongation. Some recent samples are of lower modulus.

Comparison of Different Center Blocks (Sample 727-3 Versus Sample 727-9)

The center block of sample 727-3 is B/A while that of sample 727-9 is An. The sample 727-3 shows a smaller T_m depression which seemed to be related to its larger BAMO end block sequence. The heat of melting of both samples are similar. As previously mentioned, sample 727-9 containing all its BAMO content in end blocks, shows higher heat of melting when normalized because the BAMO in the end block is usually of longer sequence length than the corresponding BAMO in the center block.

CONCLUSIONS

The preliminary analysis shows that the T_g reflects the property of the amorphous block. The presence of BAMO in the near vicinity would affect the T_g . The BAMO end blocks apparently do not effect it. The melting behaviors are determined by the BAMO sequence. Its block length and sequence regularity affect the melting. The center AMMO block also changes the melting behaviors. Examples on how the structures affect the copolymer's glass transition, melting temperature, heat of melting, rate of crystallization,

NWC TP 6945

and mechanical properties have been given. The spherulite size is associated more with the MW but the sharpness of the crystal depends more on the BAMO sequence regularity.

COMPOSITION AND CRYSTALLIZATION BY FT-IR

Melvin P. Nadler and Roxanne L. Quintana, Investigators

INTRODUCTION

This section will present the use of FT-IR to examine the crystallization kinetics of oxetane TPEs and will correlate the polymer structure, BAMO block length, MW, heat of melting, and other properties with crystallization rate. Polymer microstructure, sequence distribution, and end group analysis were obtained using NMR. Number and weight average molecular weights were obtained by GPC-LALLS, and melting points, heat of fusion, and glass transition temperatures were determined by DSC (References 27). Block identification and microstructure of oxetane TPEs using FT-IR will also be discussed.

EXPERIMENTAL SECTION

All IR spectra were obtained on a Nicolet 60SX FT-IR spectrometer. Spectra were taken at 4 cm^{-1} resolution using Happ-Genzel apodization and a mercury-cadmium-telluride liquid nitrogen cooled detector with a 400 cm^{-1} cutoff. Individual spectra were taken using 100 signal averaged scans with a measurement time of 20 seconds. Spectra versus time for slow crystallizations were acquired using a MACRO (subroutine to perform a series of FT-IR instructions), and 32 to 100 scans were signal averaged depending on the time interval. Rapid crystallizations were followed using the gas chromatography (GC) FT-IR software which collects 4 cm^{-1} spectra at 1- to 2-second intervals and 8 signal averaged scans.

Polymer samples were melted between two potassium bromide (KBr) plates using a Barnes heated cell and temperature controller to differentiate crystalline and amorphous IR bands. The Barnes cell has a large thermal mass so isothermal crystallizations could not be obtained from the melt. Most of the crystallization kinetics were obtained by following crystalline IR bands as a thin film formed on a KBr disc from a solution of the polymer in dichloro methane (DCM). This technique gives isothermal crystallization times, and rates can be calculated using the Avrami equation (References 28 through 30).

Block identification of TPE segments was performed using FT-IR subtraction methods. An absorbance spectrum of the TPE and the corresponding homopolymers was obtained from a thin film (from DCM) keeping the maximum absorbance at 0.5 ± 0.05 absorbance units. The IR spectrum of the end or center block was then subtracted from the copolymer and compared to the spectrum of the remaining block. For example, if the IR spectrum of polyAMMO is subtracted from the spectrum of a BAMO-AMMO-BAMO triblock copolymer then the resulting spectrum should be that of the

end block, polyBAMO, as long as no interaction occurs between blocks and there are no impurities in the blocks. The digital subtraction method also requires GPC data to show only one polymer is present and not a mixture of homopolymers and/or random polymers.

RESULTS AND DISCUSSION

Vibrational Assignments

Since the only difference in structure is an azidomethyl instead of a methyl on the quaternary carbon for BAMO, polyAMMO and polyBAMO have similar IR spectra. The two azidomethyl groups on BAMO are symmetric about the quaternary carbon allowing an ordered structure for polyBAMO and some degree of crystallinity. PolyAMMO does not have an ordered or isotactic structure and, therefore, is amorphous. Table 10 gives the IR frequencies and assignments for five polyoxetanes and shows how crystal field splitting (CFS) complicates the spectrum of crystalline polyBAMO. The IR spectra were obtained as follows: polyAMMO (sample 727-8) thin film, pure crystalline polyBAMO by subtraction of amorphous polyBAMO from polyBAMO; amorphous polyBAMO by heating thin film of polyBAMO (sample 726-40) above its melting point; polyBAMO (sample 726-40) thin film from DCM; and 50:50 random BAMO/AMMO from thin film of sample 646-89. Several assignments can be made from Table 10: the $\nu_a(\text{CH}_3)$ for AMMO is at 2968 cm^{-1} ; bands that occur for both crystalline polyBAMO and polyBAMO must be due to the crystalline phase; the random BAMO/AMMO (sample 646-89) shows no crystalline phase; and the spectra appear to be additive, i.e., random B/A is polyAMMO plus amorphous polyBAMO (except for minor shifts). The vibrational assignments are made from previous literature (Reference 31) and spectral correlations and are consistent with the known structures. Two bands were chosen to monitor crystalline polyBAMO: the C-O-C bend at 640 cm^{-1} (backbone vibration) and the N_3 bend at 572 cm^{-1} (pendent group vibration).

TABLE 10. Vibrational Frequencies and Assignments for BAMO and AMMO Polymers, cm^{-1} .

Suggested assignments	polyAMMO	Pure crystalline polyBAMO	Amorphous polyBAMO	PolyBAMO	50:50 Random BAMO/AMMO
$\nu_a(\text{CH}_3)$	2968				2967
$\nu(\text{CH})$	CFS- ^a	2955		2953sh	
		2933	2929	2929	2933
	CFS-		2907	2906	
	CFS-		2883	2895sh	
	2879		2872	2874	2872
	2803br	2860	2809br	2818br	2806br
		2819br			
$\nu_a(\text{N}_3)$	2100.5	2111.2	2103.8	2109	2101
$\delta(\text{CH}_2)$		1485	1486	1491	1486
		1454	1455	1454	1454sh
		1448	1443	1443	1448
$\delta(\text{CH}_3)$	CFS-	1382		1379sh	
		1376	1367	1367	1360br
	1350sh		1357br		
$\nu_s(\text{N}_3)$	CFS-	1311		1300sh	1299
		1300br	1290	1290	
	CFS-	1281br			1280sh
	1240sh		1235wsh		1255sh
	CFS-	1212		1214w	
	1209w				
$\nu_a(\text{COC})$			1178w	1178w	1178w
	CFS-	1163w			
		1138		1138	
	CFS-	1107s	1100	1103	1100
	1046	1054		1055	1045
$\nu_s(\text{COC})$	CFS-	963		961	
		968vw			
		942		940br	942
	CFS-	934		934	
	CFS-	912		912	
	883	880	906br	906	
	663br		885sh	883	886
COC bend	CFS-	640	662br	662sh	667
	615			641	
N_3 bend	CFS-	572		572	
		554	550	553	552
					553

^a CFS = crystal field splitting bands; br = broad; sh = shoulder; s = strong; w = weak; vw = very weak.

Crystallization Kinetics

Several triblock polyoxetanes, as well as, two homopolymers (polyBAMO and polyAMMO), and random BAMO/AMMO were examined during this study. The triblocks all had BAMO end blocks, but three different center blocks were used: (1) polyAMMO (B-A-B), (2) random 50:50 BAMO/AMMO (B-(B/A)-B), and (3) random 30:70 BAMO/AMMO (B-(B/A)-B). Note, this study is a combined effort (NWC and Aerojet) to prove the feasibility of a new triblock synthetic technique and to show that modern instrumental methods can characterize block copolymers; therefore, the synthetic method was not constant, but was refined based on the characterization data. Crystallization times and rates are one piece of the overall picture and Table 11 summarizes data from four characterization methods and gives the ideal triblock TPE or polyoxetane structure. Figure 26 is a typical crystallization run for B-(B/A)-B (sample 727-10) showing the normalized absorbance of the crystalline C-O-C bend at 640 cm^{-1} (A(640)) and the crystalline N₃ bend at 572 cm^{-1} (A(572)). The complete (t_c) and half ($t_{1/2}$) crystallization times in Table 11 are taken from the 640 cm^{-1} plot at the beginning of the final stage (levelling off) and at the 0.5 point, respectively (see Figure 26). The crystallization rate (r_c) and Avrami constant (n) are calculated from the Avrami equation (Equation 23) (References 28 through 30).

$$\theta = \exp(-r_c t^n) \quad (23)$$

where

- θ = the fraction of the amorphous phase (or $1-A(640)$),
- r_c = the rate constant,
- t = the crystallization time, and
- n = a constant depending upon many mechanistic factors.

Figure 27 is an Avrami plot of $\ln(-\ln[1-A(640)])$ versus $\ln(\text{time})$, the slope is the Avrami constant ($n = 1.9$), and the y-intercept is the $\ln(\text{rate constant})$ ($\ln(r_c) = -6.3$). Note, the slope is taken after the induction stage to the complete crystallization time. Examination of Figure 26 shows that crystallization from DCM takes places in stages: (1) induction period, (2) rapid growth, (3) turn over or slowing of growth, and (4) levelling off or very slow growth to perfect crystals. These stages occur at different times and rates for the C-O-C backbone vibration compared to the N₃ pendent group vibration (see Figure 26) indicating an energy barrier or mechanism change with functional group (Reference 32). This report will not examine details of the crystallization mechanism for polyoxetanes, but there are many papers available on the subject for other polymers (References 32 through 39). A paper by L. H. Sperling, and others (Reference 40), on the crystallization behavior of polyBAMO shows only one crystalline form exists, the melting range is 87 to 90°C (equilibrium melting temperature is 102°C) (Reference 26), and the percent crystallinity is 13 to 30%.

TABLE 11. TPE Data Summary.

Aerojet data		NMR data			GPC-LALLS data		DSC data			FT-IR crystallization data					
Sample	TPE type	B/A com- position, %	-BBB- %	Block factor ^a , %	Block index ^b , %	\bar{M}_n , K	\bar{M}_w/\bar{M}_n	T_m , °C	T_g , °C	ΔH_m , J/g	t_c , min	$t_{1/2}$, min	r_c	n	$\ln f_c$
646-79B	B-(B/A)-B ^c	69/31	44	35	55	81	2.8	86	-32	16	4-5	1.5	0.22	1.4	-1.5
646-91A	B-(B/A)-B	69/31	53	47	66	181	3.4	84	-36	23	3-4	0.7	2.3	0.99	0.83
646-95	B-(B/A)-B	76/24	35	20	45	59	1.2	58	-31	12	60	3.6	1.7×10^{-4}	2.3	-8.7
646-98	B-(B/A)-B	68/32	38	29	50	-	-	-	-	-	6	2.5	0.13	1.8	-2.0
646-99	B-(B/A)-B	66/34	46	39	61	56	1.2	-	-	-	4-5	2	0.21	1.9	-1.6
727-2	B-(B/A)-B ^d	53/47	34	27	67	84	1.5	84	-35	9.8	20	3	0.35	0.98	-1.0
727-3	B-(B/A)-B ^d	51/49	38	34	68	61	1.2	87	-36	15.4	4-5	1	0.76	1.2	-0.27
727-10	B-(B/A)-B	66/34	36	25	47	34	1.7	-	-	-	60	24	1.9×10^{-3}	1.9	-6.3
727-11	B-(B/A)-B	65/35	38	28	49	33	1.5	-	-	-	35	14	4.5×10^{-3}	1.9	-5.4
727-12	B-(B/A)-B	73/27	42	30	47	-	-	-	-	-	30	14	0.014	1.6	-4.3
727-17	B-(B/A)-B ^d	50/50	27	21	62	-	-	-	-	-	18	9	9.1×10^3	1.9	-4.7
727-4	B-A-B	23/77	15	13	86	60	1.2	82	-38	9.5	180	85	2.0×10^{-5}	2.3	-10.8
727-7	B-A-B	26/74	16	12	77	23	1.6	65.4	-36	11.4	50	33	8.5×10^{-4}	1.8	-7.1
727-9	B-A-B	45/55	32	26	77	38	1.2	76	-37	16	9	4.5	1.3×10^{-2}	2.4	-4.3
727-18	B-A-B	29/71	23	20	89	42	2.3	-	-	-	340	190	2.5×10^{-8}	3.2	-17.5
646-89	B/A	45/55	14	5	39	10	2.3	-	-43	-	-	2200	2.0×10^{-7}	2.0	-15.4
727-5B	B/A	52/48	25	17	45	53	1.2	78	-34	8.3	40	18	3.3×10^{-3}	1.8	-5.7
795-72	polyBAMO	100/0	100	100	100	8.5	2.6	92.2	-23	32	0.4	0.2	17.6	1.8	2.9
726-40	polyBAMO	100/0	100	100	100	-	-	-	-	-	0.27	0.13	27.1	1.8	3.3
727-8	polyAMMO	0/100	0	0	100	14.9	1.2	-	-39	-	-	-	-	-	-

^a BBB - 1/2 ABB.

^b (BBB + AAA)/total.

^c B/A Center block is 50% BAMO/50% AMMO.

^d B/A Center block is 30% BAMO/70% AMMO.

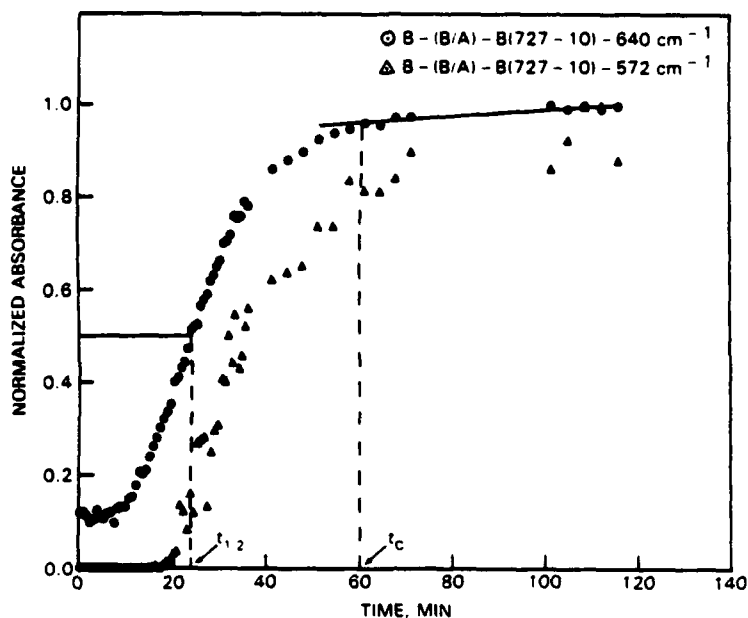


FIGURE 26. Crystallization Time Plot for 640 cm^{-1} C-O-C Bend and 572 cm^{-1} N₃ Bend From DCM.

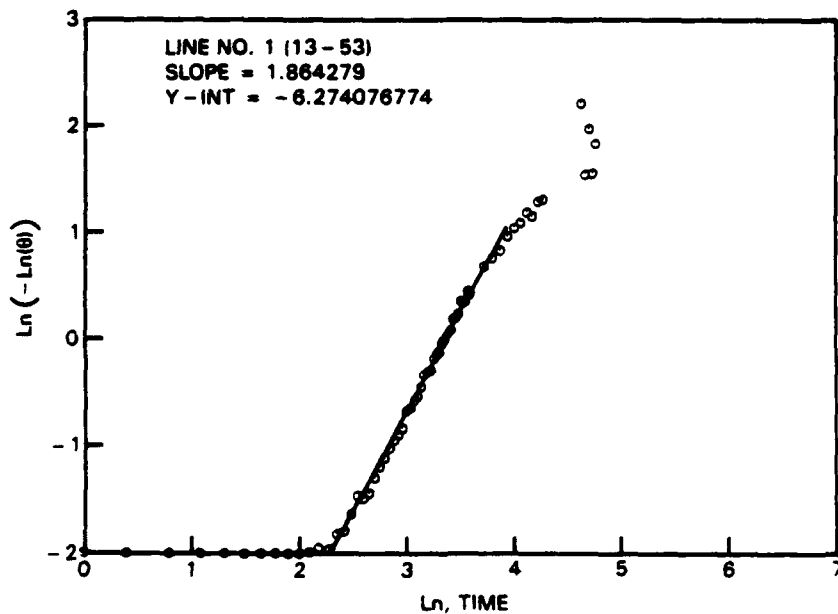


FIGURE 27. Avrami Plot for B-(B/A)-B (sample 727-10) Using the A(640).

The GPC-LALLS and DSC data in Table 11 are self explanatory, \bar{M}_n is the number average molecular weight, \bar{M}_w/\bar{M}_n is the polydispersity, T_m is the

melting temperature, T_g is the glass transition temperature, and ΔH_m is the heat of melting (for more detail see pages 31-47). However, the NMR data in Table 11 requires some explanation, percent B/A is the BAMO/AMMO percent composition determined from integration of the ^{13}C NMR, percent -BBB- is the percentage of BAMO triads, BAMO block factor ($BBB - 1/2 ABB$) corrects for the BAMO blocks in the random BAMO/AMMO and is indicative of the BAMO block length, and finally, the block index ($[(BBB + AAA)/total] \times 100$) is indicative of the "blockiness" of the block copolymer (perfect B-A-B would be 100) (for more detail see pages 17-30). The TPE type is the ideal triblock structure sought from the synthesis, and the object of this study is to come as close to the ideal structure as possible for copolymers. Note, that B-A-B (sample 727-18) has a block index of 89%, and a block index of 98% has been measured for the latest Aerojet B-A-B triblock (controlled B-A-B study of 727-20, 29, 30, 35, and 40 series to be reported at a later time.

Since the hard BAMO segment determines the crystallization behavior of these block copolymers, Figure 28 shows a plot of the BAMO block factor versus the $t_{1/2}$. Note, that $t_{1/2}$ is more precise than t_c and is related to

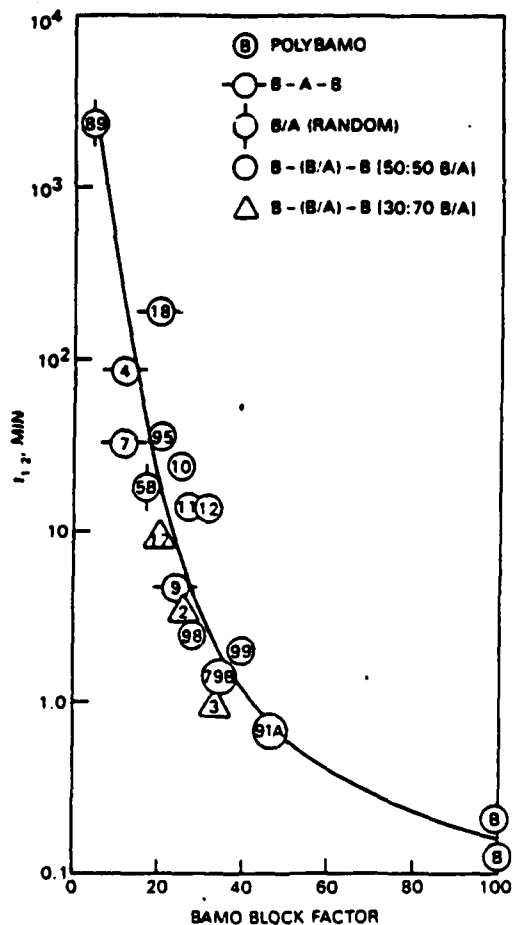


FIGURE 28. Crystallization Half-Life Versus BAMO Block Factor.

fundamental crystallization parameters (Reference 33). Figure 28 shows that, in general, the higher the BAMO block factor the faster the crystallization time, however, the spread of the data is large. Plots of percent -BBB-, percent BAMO, \bar{M}_n , or \bar{M}_w versus $t_{1/2}$ show a poorer correlation than BAMO block factor, in the order given. Figure 29 shows a plot of $t_{1/2}$ versus $\bar{M}_n \times$ (BAMO block factor/100) which is the number average BAMO block molecular weight. Copolymers that crystallize slower than the average (based on BAMO block \bar{M}_n) appear to the right of the dotted line in Figure 29 and those that are faster appear to the left. There is a dependence on BAMO \bar{M}_n for the 50:50 B/A center block copolymers but the B-A-B triblocks give greatly different $t_{1/2}$ for about the same BAMO \bar{M}_n (Figure 29). Note also that random B/A polyoxetanes (5B and 89) will crystallize (Figures 28 and 29). The BAMO block length, below which no crystallization of a triblock or copolymer can occur must be between 3 to 8 BAMO units (168 g/mol per BAMO unit), since sample 646-89 has a BAMO block \bar{M}_n of 500 to 1400 g/mol, depending upon which BAMO block percentage is used, the BAMO block factor or the -BBB- triad percentage (5 or 14%). The random copolymer sample 727-5B has a higher than expected BAMO block length for a 52:48 B/A (25% -BBB- instead of the calculated 14%) and a $t_{1/2}$ of only 18 minutes (Table 11), both of which indicate an imperfect random.

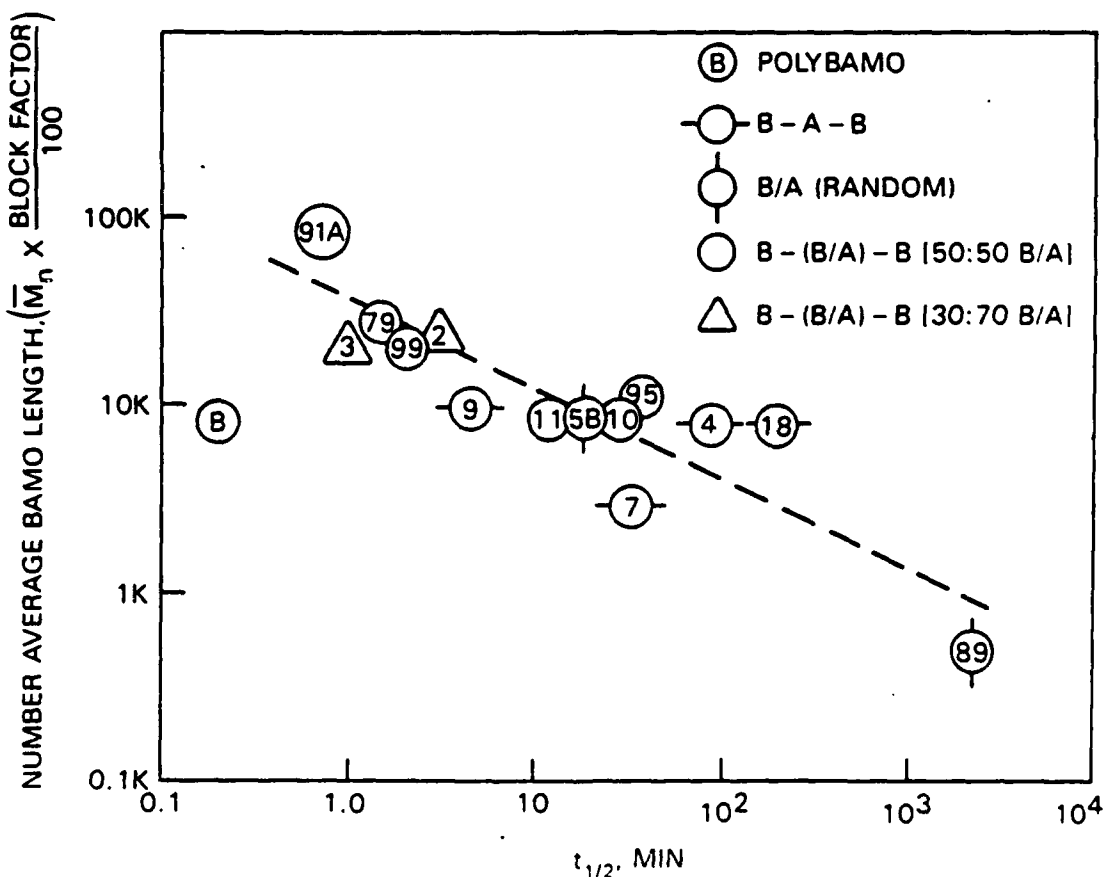


FIGURE 29. Crystallization Half-Life Versus BAMO \bar{M}_n .

Figure 30 shows a good correlation between t_c and the ΔH_m . The ΔH_m is determined from the melting point endotherm by DSC (see Table 11 and (pages 40-47)). Since DSC observed no melting point for random sample 646-89 while

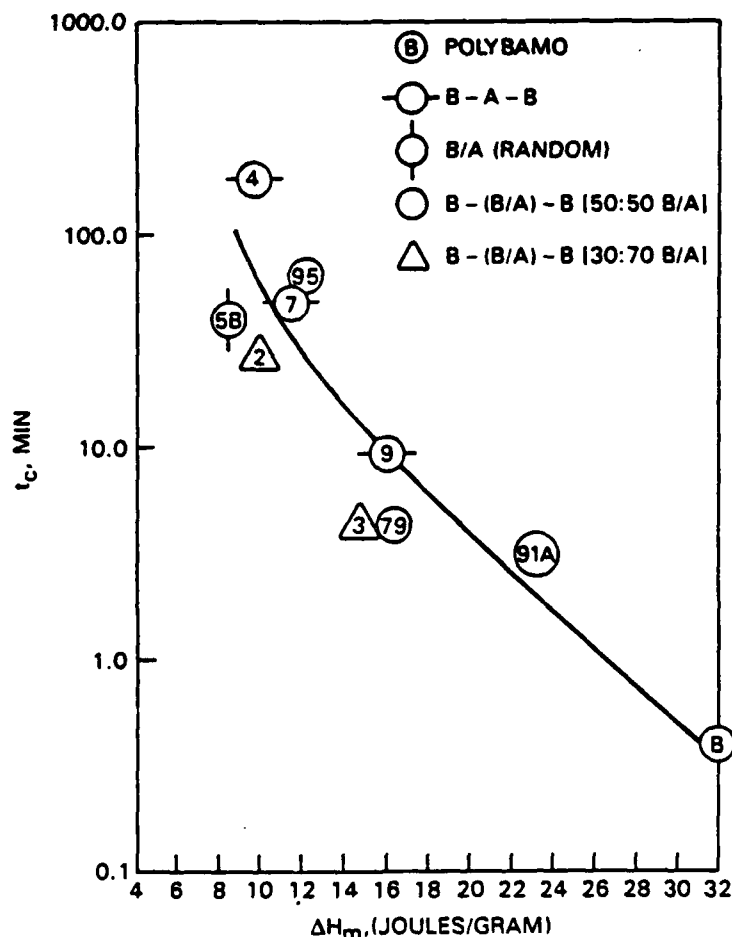


FIGURE 30. "Complete" Crystallization Time Versus Heat of Melting.

FT-IR showed crystalline bands and a $t_{1/2}$ of 2200 minutes, DSC is not as sensitive as FT-IR in determining if a copolymer has a crystalline phase. The r_c determined from the Avrami equation is plotted in Figure 31 as $\ln(r_c)$ versus the BAMO block factor. Figure 31 again shows that as BAMO block length increases the rate of crystallization increases, however, n varies from about 1 to 3 (Table 11), making comparisons of r_c unreliable. Most of the polymers tested have an n of about 2, but samples 642-91A, 727-2, and 727-3 give $n = 1$ and 727-18 gives $n = 3$ (see Table 11). The changes in n could be caused by impurities in the copolymer, since n depends on the probability of nucleation and the shape of the crystallites during growth. (References 32 and 33). It should also be noted that copolymer samples 727-2 and 727-3 have 30:70 B/A center blocks, sample 642-91A has a high MW, and sample 727-18 has

a longer than expected $t_{1/2}$. A study of B-A-B triblocks of controlled structure and MW is presently being conducted by Aerojet and NWC to determine optimum BAMO block length, microstructure, and other polymer properties of interest.

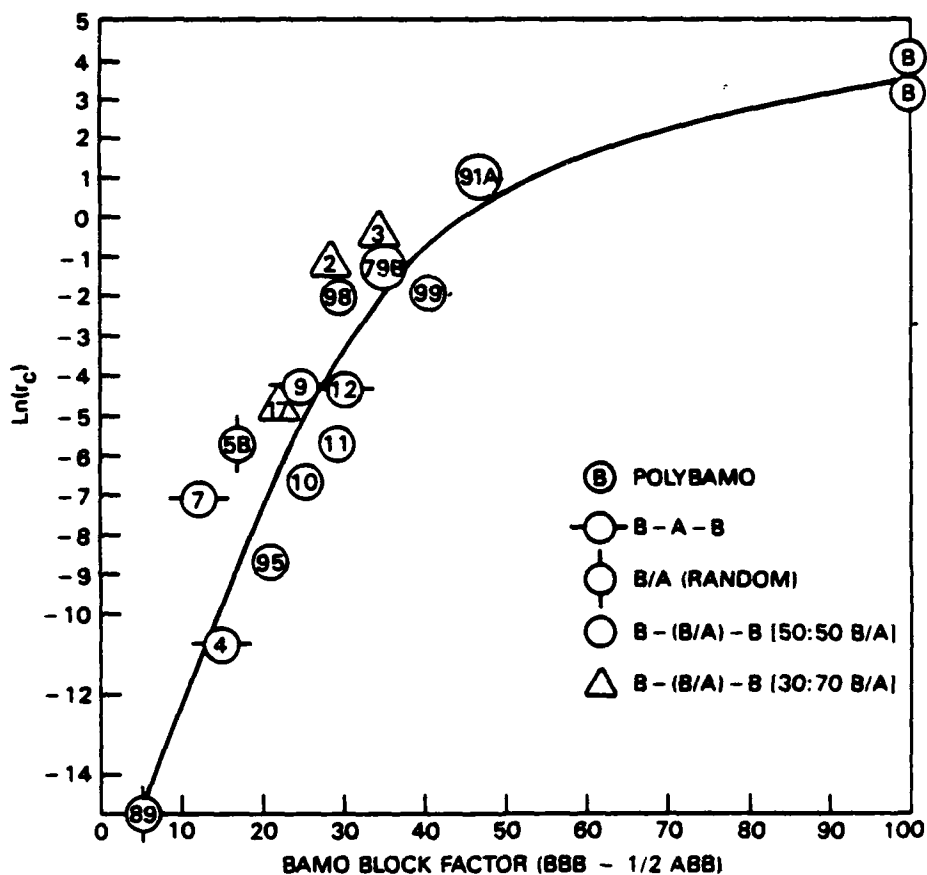


FIGURE 31. $\ln(\text{Avrami rate constant})$ Versus BAMO Block Factor.

Block Identification

Figure 32 shows an example of block identification by digital subtraction. The IR spectrum of polyBAMO is subtracted from the IR spectrum of B-A-B (sample 727-4) using the 572 cm^{-1} N_3 bend to zero-out crystalline polyBAMO and the resulting spectrum agrees with polyAMMO (Figure 32). Since GPC-LALLS data show the sample 727-4 to have a polydispersity of 1.2 (Table 11), sample 727-4 is not a mixture of polyBAMO and polyAMMO or random polymers of different molecular weights; therefore, sample 727-4 must be a block copolymer with BAMO and AMMO blocks. Some polymers showed poor agreement using the digital subtraction method, indicating a blend, a mixture of different composition polymers, impurities in the blocks, or a significant

amount of random B/A in the blocks. Nuclear magnetic resonance data show that indeed the B-A-B triblocks have some random B/A between the blocks, as indicated by the block index being less than 100 (Table 11).

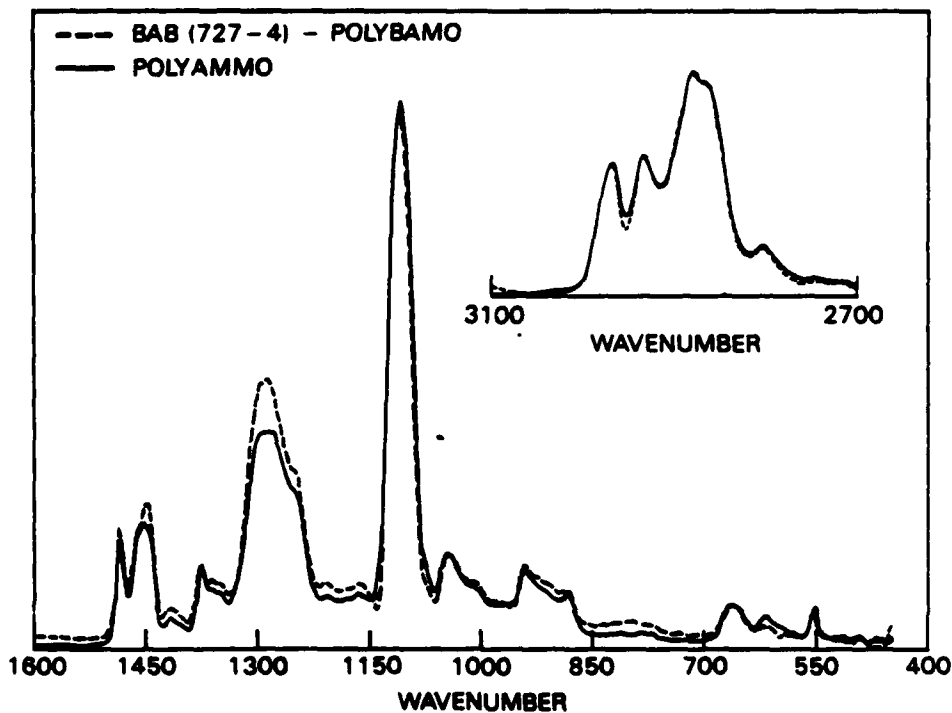


FIGURE 32. B-A-B (Sample 727-4) PolyBAMO Compared to PolyAMMO.

CONCLUSION

An FT-IR method has been developed to measure isothermal crystallization rates using milligram quantities of TPE. The crystallization rate of B-A-B and B-(B/A)-B triblocks increases with increased BAMO block length. There is also a dependence on BAMO end block MW, heat of melting, BAMO triad percent, block index (percent block present), and the type of center block. The crystallization rate is a rapid method to check the properties of block copolymers and a very sensitive technique to measure crystallinity.

SOLID ROCKET PROPELLANT I_{sp} CALCULATIONS; MECHANICAL PROPERTIES

Alice I. Atwood and Russell Reed, Investigators

INTRODUCTION

In this phase of the program, liquid curable BAMO/NMMO polymers were investigated primarily to determine their contributions to such factors as performance and mechanical properties when used as binders in high energy propellants. A new method of curing the polymers was also studied.

EXPERIMENTAL SECTION

Values of specific impulse were calculated for metallized compositions under conditions of low exit pressure, 0.69 psi (Figure 33). The BAMO/NMMO (70/30 mole ratio) formulations were compared to corresponding ones containing polyethylene glycol (PEG). BAMO/NMMO was found to be superior

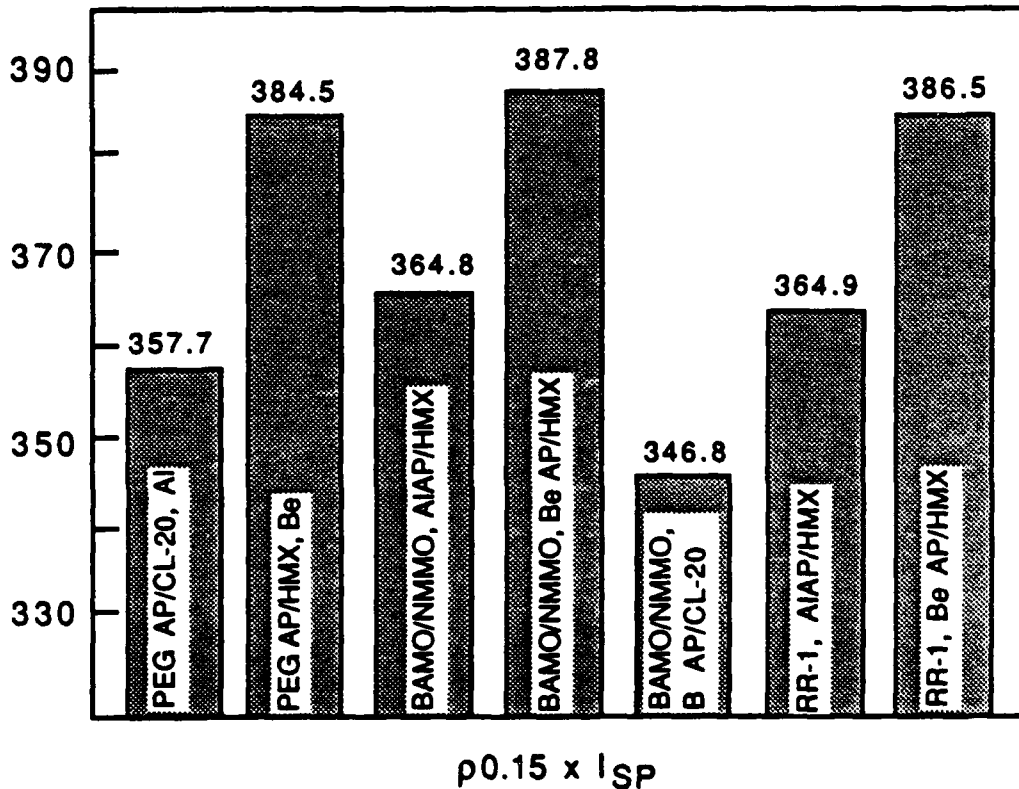


FIGURE 33. Calculated Performance of Beryllium-Containing Compositions.

to PEG in all propellant compositions. Ingredients used included the nitramines cyclotetramethylene tetranitramine (HMX), CL-20, and trinitroazetidene (TNAZ), the oxidizer ammonium perchlorate (AP), and the metals aluminum, boron, and beryllium (Be). Levels of ingredients were allowed to vary under reasonable constraints to achieve propellant compositions with an optimized specific impulse. Constraints were placed on the binder level (20 to 30% by volume) and upon the oxygen to fuel ratio (≥ 1.09). The effect of density of the compositions was taken into account by using $\rho^{0.15} \times I_{sp}$ as a measure of merit by which to judge performance. A BAMO/NMMO composition containing Be, AP, and HMX gave the highest value, 388. Formulations containing CL-20 and TNAZ were slightly lower.

Replacement of polyester binders in elastomeric modified composite double base (EMCDB) by BAMO/NMMO raises the calculated performance. High calculated performance is shown with low levels of HMX. In these calculations the nitrocellulose (NC)/BAMO-NMMO ratios were 1:1 and 1:2; butane triol trinitrate (BTTN) to total polymer was 2.5:1. At only 30% HMX, the I_{sp} was 254.5 seconds for an NC:BAMO/NMMO of 1:1 and 252.8 seconds for a ratio of 1:2. Cured propellant compositions were prepared which contained 3-nitroaza-1,5-pentane diisocyanate as the curative.

RESULTS

The evaluation of BAMO/NMMO polymers in propellant compositions continued to show that BAMO/NMMO propellants can be achieved with excellent mechanical properties that are especially high in elongation (Table 12). This property is enhanced as MW of the polymers increase; propellants containing BAMO/NMMO with a MW of 30,000 have an elongation of over 1000% but with reduced values of stress and modulus. Both stresses and moduli can be increased by increasing the BAMO content to 80%, but the elongation is then degraded as is the ability to retain plasticizer.

TABLE 12. Mechanical Properties of Trifunctional BAMO/NMMO, BTTN, and HMX (60%, 10 μ m).

Sample number	BAMO/NMMO	Molecular weight	E_o , psi	S_m , psi	ϵ_m , %	ϵ_p , %	S_{tm} , psi	Strain energy ^a
646-80	70/30	15	193	89	382	390	429	570
646-83	70/30	30	>116 ^b	68	1000	...	748	1140
646-42	80/20 ^c	15	324	97	128	132	221	208

^a lbs/in³.

^b Sample did not break.

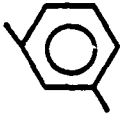
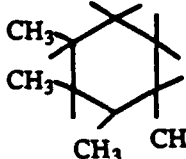
^c Exuded at $PI/P_o = 3$; data at $PI/P_o = 2$.

BAMO/NMMO propellant compositions display much less dilatation (0.5 to 1.2 volume percent) than do comparable propellants containing PEG binders (10 to 30 volume percent). Hence, BAMO/NMMO containing propellants may exhibit an enhanced degree of damage resistance in various sensitivity tests.

CONCLUSIONS

BAMO/NMMO and the binders used in current propellants are terminated in hydroxyl and are cured by reaction with isocyanates to form chain-extended and cross-linked rubbers. In contrast with the widely used PEG, BAMO/NMMO and NMMO have hydroxyl groups which are hindered and display a reduced rate of urethane formation, a process which continues to decrease as the curing proceeds. Another method of curing not involving the hydroxyl group would be desirable. The reaction of diacetylenes with the azido groups in BAMO/NMMO has been found to be a potentially useful curing technique in the case of BAMO/NMMO of relatively high MW (≥ 15 K). A variety of diacetylenes have been found to cure BAMO/NMMO-BTTN solutions and HMX containing propellant compositions (Table 13). Compositions having a ratio of C=C/branch of BAMO/NMMO of near unity displayed the best mechanical properties using trifunctional BAMO/NMMO. The triazoles formed by the cycloaddition of acetylene and azide are thermally stable and chemically inert and should be superior to the more labile urethanes. A disadvantage of the curing process is that the triazole linkages are formed randomly along the chains, thus necessitating the use of relatively long chain BAMO copolymers. However, given long chains, the curing should, in theory, give cured polymers with excellent properties.

TABLE 13. Diacetylenes Found in This Study.

Diacetylene	Source
$\text{HC}\equiv\text{C}(\text{CH}_2)_3\text{C}\equiv\text{CH}$	Columbia
$\text{NCC}\equiv\text{C}$  $\text{C}\equiv\text{CCN}$	RAH-1
$\text{HC}\equiv\text{C CO}$  $\text{COC}\equiv\text{CH}$	FHC
$\text{HC}\equiv\text{CCOOCH}_2\text{CO}(\text{CH}_2)_8\text{COCH}_2\text{OCOC}\equiv\text{CH}$	RAH-2
 $\text{NHCOOCH}_2\text{C}\equiv\text{CH}$ $\text{CH}_2\text{ NHCOOCH}_2\text{C}\equiv\text{CH}$	RAH
$\text{HC}\equiv\text{C CH}_2\text{O CO NH CH}_2\text{C}(\text{NO}_2)_2\text{CH}_2\text{NHCOOCH}_2\text{C}\equiv\text{CH}$	RR

REFERENCES

1. Morton Thiokol, *High Energy Binders, Final Report*, by G. E. Manser, R. W. Fletcher and M. R. Knight. Brigham City, Utah, Morton Thiokol, Inc., Wasatch Division, June 1985 (PROJECT JM101, Paper UNCLASSIFIED).
2. J. P. Kennedy. *Cationic Polymerization of Olefins: A Critical Inventory*, Institute of Polymer Science, The University of Akron, Wiley Interscience Publication, 1975.
3. M. Sawamoto and J. P. Kennedy. "Quasiliving Carbocationic Polymerization of Vinyl Ether," *Am. Chem. Soc., Polym. Preprints*, Vol. 22(2) (1981), pp. 140-41.
4. J. P. Kennedy and R. A. Smith. "New Telechelic Polymers and Sequential Copolymers by Polyfunctional Initiators-Transfer Agents Inifers. II. Synthesis and Characterization of α,ω -di(tert-chloro)polyisobutylenes," *J. Polym. Sci.*, Vol. 18 (1980), pp. 1523-37.
5. R. Faust, A. Fahervari, and J. P. Kennedy. "New Telechelic Polymers and Sequential Copolymers by Polyfunctional Initiator-Transfer Agents Inifers. XXXIX. Semicontinuous Preparation of End-Reactive Isobutylene Oligomers by the Inifer Technique," *Am. Chem. Soc., Polym. Preprints*, Vol. 25(1) (1984), pp. 133-34.
6. B. Ivan, J. P. Kennedy, and V. S. C. Chang. "New Telechelic Polymers and Sequential Copolymers by Polyfunctional Initiator-Transfer Agents Inifers. VII. Synthesis and Characterization of α,ω -(dihydroxy)-polyisobutylene," *J. Polym. Sci.*, Vol. 18 (1980), pp. 3177-91.
7. S. Aoshima, T. Nakamura, N. Uesugi, M. Sawamoto, and T. Higashimura. "Living Cationic Polymerization of Vinyl Ethers With a Functional Group. 1. Polymerization of 2-Acetoxyethyl Vinyl Ether and Synthesis of Polyalcohols With a Narrow Molecular Weight Distribution," *Macromolecules*, Vol. 18 (1985), pp. 2097-101.
8. (a) J. C. Randall. "Carbon-13 NMR in Polymer Science," in *ACS Symposium Series*, ed. by W. M. Pasika, Washington, DC, American Chemical Society; Vol. 103, 1979. Pp. 291-313.
(b) Jacob Schaefer, "The Carbon-13 NMR Analysis of Synthetic High Polymers" in *Topics in ^{13}C NMR Spectroscopy*, Vol. 1, ed. by G. C. Levy. New York, Wiley, 1974. Pp. 149-208.
9. M. I. Martin, J. -J. Delpuech, and G. J. Martin, "Practical NMR Spectroscopy," Philadelphia, Heyden, 1980. Pp. 122-24.
10. A. E. Derome, "Modern NMR Techniques for Chemistry Research." Vol. 6, ed. by J. E. Baldwin, New York, Pergamon, 1987. Pp. 143-52.

11. W. H. Stockmayer, L. D. Moore, M. Fixman, and B. N. Epstein, Copolymers in Dilute Solution. I. Preliminary Results for Styrene-Methyl Methacrylate, *J. Polym. Sci.*, Vol. 16 (1955), Pp. 517-30.
12. W. Bushuk and H. Benoit, Light-Scattering Studies of Copolymers. 1. Effect of Heterogeneity of Chain Composition on the Molecular Weight, *Can. J. Chem.*, Vol. 36, (1958), pp. 1616-26.
13. H. Benoit and D. Froelich, *Light Scattering From Polymer Solutions*. M. B. Huglin, ed. New York, Academic Press, 1972. Pp. 467-501.
14. M. B. Malihi, C. Y. Kuo, and T. Provder, Determination of the Absolute Molecular Weight of a Styrene-Butyl Acrylate Emulsion Copolymer by Low-Angle Laser Light Scattering (LALLS) and GPC/LALLS, *J. Appl. Polym. Sci.*, Vol. 29 (1984), 925-31.
15. R. C. Jordan and M. L. McConnell. Characterization of Branched Polymers by Size Exclusion Chromatography With Light Scattering Detection in *Proceedings, ACS Symposium*, 1980, pp. 107-29.
16. K. Kamide, A. Kiguchi, and Y. Miyazaki, Viscometric and Light Scattering Study in Dimethylacetamide of Linear Segment Polyurethane, Polymerized With Methylene bis(4-phenyl isocyanate), Polytetra-methylene Glycol and Ethylene Diamine, *Polym. J.*, Vol. 18(12) (1986), pp. 919-25.
17. W. Kaye, Low-Angle Laser Light Scattering, *Anal. Chem.*, Vol. 45(2) (1973), pp. 221A-25A.
18. M. L. McConnell, Polymer Molecular Weights and Molecular Weight Distributions by Low-Angle Laser light Scattering, *Am. Lab.*, Vol. 63 (May 1978), pp. 63-75.
19. V. Grinshpun and A. Rudin, A New Method for Determining Molecular Weight Distributions of Copolymers, *J. Appl. Polym. Sci.*, Vol. 32 (1986), pp. 4303-11.
20. R. C. Jordan, S. F. Silver, R. D. Schon, and R. J. Rivard. Size Exclusion Chromatography With Low-Angle Laser Light-Scattering Detection. Application to Linear and Branched Block Copolymers in *Proceedings, ACS Symposium*, 1984, pp. 295-320.
21. M. Gordon and J. S. Taylor, Ideal Copolymers and the Second-Order Transitions of Synthetic Rubbers. I. Non-Crystalline Copolymer, *J. Appl. Chem.*, Vol. 2 (1952), pp. 493-500.
22. R. F. Fedors, A Simple Model for the Virtually Crosslinked Block Copolymers, *J. Poly. Sci.*, C26 (1969), pp. 189-99 .

23. B. D. Nahlovsky, "Synthetic Thermoplastic Elastomers for Solid Propellant Binders," in *Proceedings of the 1987 JANNAF Propulsion Meeting, San Diego, Calif, 15-17 December 1987*. Laurel, Md., Chemical Propulsion Information Agency (in press). Publication UNCLASSIFIED.
24. P. J. Flory, Thermodynamics Crystallization in High Polymers. IV. A Theory of Crystalline Slaters and Fusins in Polymers, Copolymers, and Their Mixtures with Diluents, *J. Chem. Phys.*, Vol. 17 (1949), pp. 223-40.
25. P. J. Flory, Theory of Crystallization in Copolymers, *Trans. Faraday Soc.*, Vol. 51 (1955), pp. 848-57.
26. C. J. Murphy, G. V. S. Henderson, Jr., E. A. Murphy, and L. H. Sperling, The Relationship Between the Equilibrium Melting Temperature and the Supermolecular Structure of Several Polyoxetanes and Polyethylene Oxides, *Poly. Eng. and Sci.*, Vol. 27 (1987), pp. 781-87.
27. R. A. Nissan and R. J. Cramer, "Equivalent Weight and Functionality Determinations of Polyols by Trifluoroacetylation and ^{19}F NMR Analysis," in *Proceedings of the 1986 JANNAF Propellant Characterization Subcommittee Meeting, Monterey, California., November 1986*. Laurel, Md., Chemical Propulsion Information Agency, pp. 117-23. (92839 N86, publication UNCLASSIFIED.)
28. M. Avrami, *J. Chem. Phys.*, Vol. 7 (1939), pp. 1103.
29. M. Avrami, *J. Chem. Phys.*, Vol. 8 (1940), pp. 212.
30. M. Avrami, *J. Chem. Phys.*, Vol. 9 (1941), pp. 177
31. Y. Oyumi and T. B. Brill, On the Lineshape of $\nu_{\text{as}}(\text{NO}_2)$ in Nitrate Esters: 3,3-bis(nitratomethyl)oxetane, *Spectrochim. Acta*, Vol. 42A(9) (1986), pp. 1001-04.
32. B. J. Bulkin, M. Lewin, and M. L. McKelvy, Crystallization Kinetics of PET Studied by Rapid Scanning Raman Spectroscopy, *Spectrochim. Acta*, Vol. 41A(1/2) (1985), pp. 251-61.
33. K. Sawada and Y. Ishida, Dielectric Study of Crystallization in poly-(ethylene terephthalate), *J. Polym. Sci., Polym. Phys. Ed.*, Vol. 13 (1975), pp. 2247-50.
34. T. Yu, H. Bu, and J. Chen, The Effect of Units Derived from Diethylene Glycol on Crystallization Kinetics of PET, *Makromol. Chem.*, Vol. 187 (1986), pp. 2697-709.

35. F. Van Antwerpen and D. W. Van Krevelen, Influence of Crystallization Temperature, Molecular Weight, and Additives on Crystallization Kinetics of Poly(ethylene Terephthalate), *J. Polym. Sci., Polym. Phys. Ed.*, Vol. 10 (1972), pp. 2423-35.
36. G. Groeninckx, H. Berghmans, N. Overbergh, and G. Smets, Crystallization of PET Induced by Inorganic Compounds, *J. Polym. Sci., Polym. Phys. Ed.*, Vol. 12 (1974), pp. 303-16.
37. Shaow-Burn Lin and J. L. Koenig, A Kinetic Analysis of the Gouche-Transisomerization in Semicrystalline PET, *J. Polymer Sci., Polym. Phys. Ed.*, Vol. 21 (1983), pp. 2365-78.
38. Tong Sun, Jose Pereira, and R. S. Porter, Crystallization Kinetics for PET Oriented by Solid-State Coextrusion, *J. Polym. Sci., Polymer Phys. Ed.*, Vol. 22 (1984), pp. 1163-71.
39. A. Misra and R. S. Stein, Light Scattering Study of the Early Stages of the Crystallization of PET, *Polym. Lett.*, Vol. 10 (1972), pp. 473-77.
40. K. E. Hardenstine, G. V. S. Henderson, Jr., L. H. Sperling, C. J. Murphy, and G. E. Manser, Crystallization Behavior of Poly(3,3-bis-ethoxymethyl Oxetane) and Poly(3,3-bis-azidomethyl Oxetane), *Polym. Sci., Polym. Phys. Ed.*, Vol. 23 (1985), pp. 1597-609.

INITIAL DISTRIBUTION

- 3 Naval Air Systems Command
 - AIR-5004 (2)
 - AIR-932F, B. Sobers
- 10 Chief of Naval Research, Arlington (OCNR-432P, Dr. R. S. Miller)
- 4 Naval Sea Systems Command
 - SEA-09B312 (2)
 - SEA-96R, Dr. J. Pastine (1)
 - SEA-D3, C. M. Christensen (1)
- 1 Commander in Chief, U. S. Pacific Fleet, Pearl Harbor (Code 325)
- 1 Headquarters, U. S. Marine Corps (Code RD-1, A. L. Slafkosky)
- 1 Commander, Third Fleet, San Francisco
- 1 Commander, Seventh Fleet, San Francisco
- 2 Naval Academy, Annapolis (Director of Research)
- 1 Naval Explosive Ordnance Disposal Technology Center, Indian Head (Code D. L. Dickinson)
- 2 Naval Ordnance Station, Indian Head
 - Code 5253, W. G. Roger (1)
 - Code 5253K, J. A. Birkett (1)
- 1 Naval Postgraduate School, Monterey (Code 012, Dr. J. Wall)
- 1 Naval Research Laboratory (Code 6120, Dr. W. Moniz)
- 1 Naval Surface Warfare Center, Indian Head Detachment, Indian Head (Code R16, J. Consaga)
- 8 Naval Surface Center, White Oak Laboratory, Silver Spring
 - Code R10B, M. J. Stosz (1)
 - Code R10C, L. A. Roslund (1)
 - Code R10E, J. M. Kelley (1)
 - Code R11
 - Dr. H. G. Adolph (1)
 - J. Goldwasser (1)
 - C. Gotzmer (1)
 - K. F. Mueller (1)
 - J. M. Short (1)
- 1 Naval War College, Newport
- 2 Naval Weapons Support Center, Crane
 - Code 5063, Dr. H. Webster III (1)
 - A. Chen (1)
- 2 Office of Naval Technology, Arlington
 - ONT-07CI, Dr. L. V. Schmidt (1)
 - ONT-21, Dr. E. Zimet (1)
- 2 Strategic Systems Project Office
 - SSPO/SP-2731
 - J. M. Culver (1)
 - E. L. Throckmorton (1)
- 2 Army Missile Command, Redstone Arsenal
 - ARMSI-RD-PR-L, P. H. Mitchell (1)
 - DRSMI-RKL, W. W. Wharton (1)
- 1 Army Armament Research, Development and Engineering Center, Picatinny Arsenal (DRSMC-LCE)
- 1 Army Ballistic Missile Defense Advanced Technology Center, Huntsville (D. C. Sayles)
- 3 Army Ballistic Research Laboratory, Aberdeen Proving Ground
 - DRXBR-IBD
 - Director (1)
 - Dr. I. W. May (1)
 - J. J. Rocchio (1)
- 2 Army Research Office, Research Triangle Park
 - Chemical and Biological Sciences Division (1)
 - Engineering Division, Dr. D. Mann (1)

NWC TP 6945

- 1 Air Force Academy, Colorado Springs (FJSRL/NC, J. S. Wilkes, Jr.)
- 1 Air Force Armament Division, Eglin Air Force Base (AFATL/FXG)
- 1 Air Force Intelligence Agency, Bolling Air Force Base (AFIA/INTAW, Maj. R. Esaw)
- 3 Air Force Office of Scientific Research, Bolling Air Force Base
 - Directorate of Aerospace Sciences, L. H. Caveny (1)
 - Directorate of Chemical and Atmospheric Sciences
 - Dr. D. L. Ball (1)
 - Dr. A. J. Matuszko (1)
- 4 Air Force Astronautics Laboratory, Edwards Air Force Base
 - AFAL/DY
 - R. Geisler (1)
 - M. Irwin (1)
 - C. Merrill (1)
 - F. Roberto (1)
- 2 Defense Technical Information Center, Alexandria
- 1 Lawrence Livermore National Laboratory, University of California, Livermore, CA
 - (Code L324, R. McGuire)
- 2 Los Alamos National Laboratory, Los Alamos, NM
 - INC-4, B. Swanson (1)
 - T-3. B216, Dr. J. K. Dienes (1)
- 2 Aerojet Solid Propulsion Company, Sacramento, CA
 - Dr. R. L. Lou (1)
 - G. Manser (1)
- 1 Aerojet Tactical Systems, Sacramento, CA (G. A. Zimmerman)
- 1 Atlantic Research Corporation, Alexandria, VA (M. K. King)
- 5 Atlantic Research Corporation, Gainesville, VA
 - M. Barnes (1)
 - G. T. Bowman (1)
 - R. E. Shenton (1)
 - W. Waasche (1)
 - B. Wheatley (1)
- 1 Dr. M. Farber, Monrovia, CA
- 1 Georgia Institute of Technology, School of Aerospace Engineering, Atlanta, GA
 - (Prof. E. Price)
- 2 Hercules Incorporated, Allegany Ballistics Laboratory, Rocket Center, WV
 - Aerospace Division
 - Dr. A. Defusco (1)
 - Dr. K. D. Hartman (1)
- 2 Hercules Incorporated, Magna, UT
 - G. Butcher (1)
 - Dr. R. Earl (1)
- 2 Lockheed Missiles and Space Company, Sunnyvale, CA (via NAVPRO)
 - G. A. Lo (1)
 - Dr. R. Martinson (1)
- 2 Massachusetts Institute of Technology, Department of Chemistry, Cambridge, MA
 - Prof. R. Brown (1)
 - Prof. J. Deutch (1)
- 1 Morton-Thiokol, Incorporated, Aerospace Group, Chicago, IL (Dr. T. F. Davidson)
- 1 Morton-Thiokol, Incorporated, Aerospace Group, Ogden, UT (D. A. Flanigan)
- 1 Morton-Thiokol, Incorporated, Elkton Division, Elkton, MD (Dr. R. Willer)
- 1 Morton-Thiokol, Incorporated, Huntsville Division, Huntsville, AL (Dr. R. B. Kruse)
- 1 Morton-Thiokol, Incorporated, Longhorn Division, Marshall, TX (Dr. D. Dillehay)
- 2 Morton-Thiokol, Incorporated, Shreveport, LA
 - L. C. Estabrook (1)
 - Dr. J. R. West (1)
- 2 Morton-Thiokol, Incorporated, Wasatch Division, Brigham City, UT (via AFPRO)
 - J. Hinshaw (1)
 - G. Thompson (1)
- 1 P. A. Miller, San Francisco, CA
- 1 Pennsylvania State University, Department of Mechanical Engineering, University Park, PA (Prof. K. Kuo)
- 2 Rockwell International Corporation, Rocketdyne Division, Canoga Park, CA
 - M. Frankle (1)
 - E. Wilson (1)
- 1 Rutgers University, High Pressure Materials Research Laboratory, Piscataway, NJ
 - (K. D. Pae)

NWC TP 6945

- 3 SRI International, Menlo Park, CA
 - D. Curran (1)
 - J. T. Rosenberg (1)
 - Dr. D. A. Shockey (1)
- 1 Texas A&M University, Civil Engineering Department, College Station, TX (R. Schapery)
- 2 The John Hopkins University, Laurel, MD
 - Chemical Propulsion Information Agency, T. W. Christian (1)
 - Department of Chemistry, Dr. J. Kaufman (1)
- 1 United Technologies Corporation, Chemical Systems Division, San Jose, CA
 - (Dr. R. S. Valentine)
- 1 University of Akron, Institute of Polymer Science, Akron, OH (A. N. Gent)
- 1 University of California, Department of Chemistry and Biochemistry, Los Angeles, CA
 - (Prof. M. Nicol)
- 2 University of Maryland, Department of Mechanical Engineering, College Park, MD
 - Prof. R. W. Armstrong (1)
 - R. G. Rosemier (1)
- 3 Washington State University, Department of Physics, Pullman, WA
 - J. T. Dickinson (1)
 - G. D. Duvall (1)
 - M. H. Miles (1)